A cell fate decision map reveals abundant direct neurogenesis bypassing intermediate progenitors in the human developing neocortex

Laure Coquand, Clarisse Brunet Avalos, Anne-Sophie Macé, Sarah Farcy, Amandine Di Cicco, Marusa Lampic, Ryszard Wimmer, Betina Bessières, Tania Attie-Bitach, Vincent Fraisier, et al.

A cell fate decision map reveals abundant direct neurogenesis in the human developing neocortex

Laure Coquand[1*], Clarisse Brunet Avalos[1*], Anne-Sophie Macé[2], Sarah Farcy[1], Amandine Di Cicco[1], Marusa Lampic[1], Ryszard Wimmer[1], Betina Bessières[3], Tania Attie-Bitach[3], Vincent Fraisier[2], Pierre Sens[4], Fabien Guimiot[5], Jean-Baptiste Brault[1], Alexandre Baffet[1, 6, 7]

1- Institut Curie, PSL Research University, CNRS UMR144, Paris, France
2- UMR 144-Cell and Tissue Imaging Facility (PICT-IBiSA), CNRS-Institut Curie, Paris, France.
3- UF Embryofœtopathologie, Hopital Necker-enfants malades, Paris, France
4- Institut Curie, PSL Research University, CNRS UMR168, Paris, France
5- UF de Fœtopathologie – Université de Paris et Inserm UMR1141, Hôpital Robert Debré, Paris, France
6- Institut national de la santé et de la recherche médicale (Inserm)
7- alexandre.baffet@curie.fr
*These authors contributed equally

Abstract

The human neocortex has undergone strong evolutionary expansion, largely due to an increased progenitor population, the basal radial glial (bRG) cells. These cells are responsible for the production of a diversity of cell types, but the successive cell fate decisions taken by individual progenitors remain unknown. Here, we developed a semi-automated live/fixed correlative imaging method to map bRG cell division modes in early fetal tissue and cerebral organoids. Through the live analysis of hundreds of dividing progenitors, we show that bRG cells undergo abundant symmetric amplifying divisions, and frequent self-consuming direct neurogenic divisions, bypassing intermediate progenitors. These direct neurogenic divisions are more abundant in the upper part of the subventricular zone. We furthermore demonstrate asymmetric Notch activation in the self-renewing daughter cells, independently of basal fiber inheritance. Our results reveal a remarkable conservation of fate decisions in cerebral organoids, supporting their value as models of early human neurogenesis.

Introduction

The human neocortex, composed of billions of neuronal and glial cells, is at the basis of higher cognitive functions[1]. Its evolutionary size expansion is particularly important in the upper layers, leading to increased surface area and folding[2]. This is largely due to progenitor cells called basal radial glial cells (bRGs), also known as outer radial glial cells[3-6]. These cells are highly abundant in humans - but rare in mice[7,8] – and reside in the outer subventricular zone (OSVZ) where they may contribute to the majority of supragranular neurons[9].

bRG cells derive from apical (also known as ventricular) RG cells but have lost their connection to the ventricular surface through a process resembling an epithelial-mesenchymal transition (EMT) (Fig. 1a)[10,11]. A major feature of bRG cells is the presence of an elongated basal process along which newborn neurons migrate, though various morphologies have been reported including the presence of an apical process that does not reach the ventricle[12]. bRG cells express various RG markers such as PAX6, Vimentin and SOX2, and undergo an unusual form of migration called mitotic somal translocation (MST) which occurs shortly before cytokinesis[13]. Consistent with a steady increase of the bRG cell pool during development, live imaging experiments have documented their high proliferative potential[4,5,12]. bRG cells are believed to increase the neurogenic output of the cortex while providing extra tracks for radial migration and tangential dispersion of neurons[14].

Genomic analyses have revealed the transcriptional profile of bRG cells as well as the cellular diversity in the human developing neocortex[15-17]. They highlighted the conservation of cellular identities between fetal tissue and cerebral organoids, despite some degree of metabolic stress[18-23]. Such studies led to the identification of several human bRG-specific genes with important roles in bRG cell generation and amplification[16,24-26]. These methods nevertheless do not allow to identify the cell fate decisions taken at the single progenitor level that lead to this diversity[27,28]. Indeed, the sequence of progenitor divisions cannot be predicted from their final cellular output[29]. Identifying these progenitor cell fate decision modes (i.e. the fate of two daughter cells) is critical to understand how neurogenesis is regulated across species, and affected in pathological contexts. Before gliogenic stages, bRG cells can, theoretically, undergo several division modes: symmetric proliferative (two RG daughters), symmetric self-consuming (two differentiating daughters), or asymmetric self-renewing divisions (one RG and one differentiating daughter). Moreover, differentiating divisions can lead to the production of a neuron (direct neurogenic division) or an intermediate progenitor (IP, indirect neurogenic division).

Here, we developed a method to quantitatively map human bRG cell division modes. Using a semi-automated live-fixed correlative imaging approach that enables bRG daughter cell fate identification following division, in space and in time, we have established a map of cell fate decisions in human fetal tissue and cerebral organoids. We observe a remarkable similarity of division modes between the two tissues, and identify two remarkable behaviors: abundant symmetric amplifying divisions, as well as frequent self-consuming direct neurogenic divisions, suggesting an alternative route to the asymmetric self-renewing divisions which dominate in mouse aRG cells. Within these asymmetrically dividing cells, we demonstrate that basal process inheritance does not correlate with asymmetric NOTCH signaling and self-renewal, and is a consequence rather than a cause of bRG cell fate.

Results

Morphological identification of bRG cells

To identify human bRG cell division modes using live imaging methods, we first validated the identification of these cells based on morphological features. Human fetal pre-frontal cortex tissues from Gestational Week (GW) 14-18 were stained for phospho-Vimentin, which marks mitotic RG cells. Imaging within the SVZ revealed four different morphologies for these cells: unipolar with a single apical process (not reaching the VZ), unipolar with a basal process, bipolar with both an apical and a basal process, and cells with no visible process (Fig. 1b, c). Mitotic bipolar bRG cells always had a major thick process and a minor thin process, which could be apical or basal (Fig. 1b, 2P). Overall, over 80% p-VIM+ cells displayed at least one process, and 60% a basal process. All process-harboring p-VIM+ cells were also SOX2+, while 20% of non-polarized p-VIM+ cells were negative for SOX2 (Fig. 1d).

We then explored bRG cell morphology in non-mitotic cells. We first validated bRG identity by showing that they were positive for HOPX and SOX2 (RG cells), but negative for EOMES (IPs), and HuC/D and NEUN (Neurons) (Extended Data Fig. 1a, b). Fetal brain slices were infected with GFP-expressing retroviruses (RV) and stained for SOX2, EOMES, and NEUN (Fig. 1e and Extended Data Fig. 1c, d). This analysis confirmed that over 80% of SOX2+/EOMES-/NEUN- cells displayed apical and/or basal processes, while 20% were non-polarized (Fig. 1f, g). Moreover, the majority of process-harboring cells were SOX2+/EOMES-/NEUN-, and around 40% of non-polarized cells were SOX2+/EOMES-/NEUN- (Fig. 1h). Therefore, human fetal bRG cells largely display elongated processes, though 20% are non-polarized.

We next performed live imaging of GFP-expressing cells in fetal slices, focusing on elongated bRG cells. Dividing cells had the same morphology as previously described in fixed samples (Extended Data Fig. 1e). The majority of process-harboring cells performed MST, though 25% performed stationary divisions (Fig. 1i, j and Supplementary Video 1). MST could occur in the apical direction or the basal direction, depending on their shape. When bRG cells had two processes, MST occurred in the dominant (thick) process (Fig. 1j).

Finally, we asked whether these morphological features were conserved in dorsal forebrain organoids. Week 8-10 organoids were infected with RV and stained for the cell fate marker SOX2, EOMES and NEUN, which revealed abundant SOX2+ bRG cells above the ventricular zone (Fig. 1k and Extended Data Fig 1f, g). As in fetal tissue, the majority of SOX2+/EOMES-/NEUN- cells displayed one or two elongated processes, and 20% were non-polarized (Fig. 1l, m). It was not possible to unambiguously identify whether processes were apical or basal, as bRG cells were often located between two lumens. The vast majority of process-harboring cells, and around 40% of non-polarized cells, were SOX2+/EOMES-/NEUN- (Fig. 1n). Live imaging confirmed these morphologies and indicated that the majority of bRG cells performed MST (Fig. 1o and Extended Data Fig 1h). Therefore, the majority of human bRG cells can be identified in live samples based on their elongated morphology and ability to divide, which is conserved between fetal tissue and organoids.

A semi-automated correlative imaging method to identify cell fate decisions.

We next developed a method to identify the fate acquired by daughter cells following progenitor cell division in cerebral organoids. We established a correlative imaging method consisting in live imaging GFP-expressing progenitors and, following fixation and immunostaining, assigning a fate to the live imaged cells (Fig. 2a). The identification of corresponding cells between the live and fixed samples can be particularly challenging as the tissue is complex and multiple slices are imaged in parallel in up to 4 dishes (60-70 videos per acquisition). Moreover, slices rotate and even flip during the immunostaining process. We therefore developed a computer-assisted method to automate the localization of the videos in the immunostained samples (see methods). In brief, RV-infected tissue slices are live imaged for 48 hours and, at the end of the movie, 4X brightfield images of the slices containing positional information from each video are generated (Fig. 2b and Supplementary Video 2). Slices are then fixed, stained for the cell fate markers SOX2, EOMES, and NEUN, and mosaic (tiled) images of the entire slices are acquired. Both live and fixed images are automatically segmented, paired, flipped and aligned. The position of each video is thereby obtained on the

immunostained images, leading to the identification of matching cells between the live and fixed samples (Fig. 2b). Using this method, dividing bRG cells can be live imaged and the fate of the two daughter cells identified (Fig. 2c and Supplementary Video 3). Daughter cell fate was analyzed on average 30 hours after division. We noted that when a daughter cell differentiated (e.g. into an EOMES+ IP), it often retained some expression of the mother cell fate marker (SOX2), irrespective of the division mode (Fig. 2c). Expression of a novel fate marker was on the contrary very rapid, with EOMES or NEUN being detected in daughter cells that had divided 1-2 hours before the end of the movie (Extended Data Fig. 2a). Moreover, putative IPs and migrating neurons can be live imaged and cell fate analyzed at the last timepoint (Fig. 2d, e and Supplementary Videos 4, 5). Therefore, this semi-automated correlative microscopy method allows the identification of cell fate markers in live imaged cerebral organoids, in a highly reproducible and quantitative manner.

A map of cell fate decisions in cerebral organoids

To generate a map of progenitor division modes, we analyzed 1,101 dividing bRG cells, in weeks 7 to 9 and 13 to 15 cerebral organoids, prior to the start of gliogenesis[18,20] (Fig. 3a, extended data Fig. 2b, c, and Supplementary Videos 6, 7, 8). We report the relative probabilities, through time, of all possible division modes: generation of (a) 2 bRGs; (b) 2 IPs; (c) 2 neurons; (d) 1 bRG and 1 IP; and (e) 1 bRG and 1 neuron (Fig. 3b for week 8, and extended data Fig. 3 for all other stages). Notably, we never observe asymmetrically dividing bRG cells generating one IP and one neuron. We first quantified the fraction of proliferative (amplifying) divisions (leading to two SOX2+ cells) versus neurogenic divisions (leading to at least one differentiating cell, EOMES+ or NEUN+). This analysis revealed a high rate of bRG cell amplification, which increases between weeks 7 and 9, and decreases between weeks 13 and 15 (Fig. 3c). Within neurogenic divisions, different patterns could be observed. bRG cells performed symmetric self-consuming divisions, leading to two differentiating cells, or asymmetric self-renewing divisions, leading to one bRG cell and one differentiating cell. Self-consuming divisions decreased between weeks 7 and 9 and increased between weeks 13 and 15 (Fig. 3d). In both types of neurogenic divisions (asymmetric or symmetric), bRG cells could divide directly into neurons or indirectly, via the generation of IPs. Strikingly, we observed that direct neurogenic divisions dominated in human bRG cells, indicating that the generation of IPs is not a systematic differentiation trajectory in these cells (Fig. 3e). These divisions decreased between weeks 7 and 9 and increased between weeks 13 and 15 (Fig. 3e).

We next modeled how these different modes of progenitor divisions affected their final output (see methods). At each stage, we predicted the average number of bRG cells, IPs and neurons generated from a single bRG cell, after four rounds of division, which corresponds to approximately 1 week of development (Fig. 3f for week 8 and extended data Fig. 4a for all other stages). At week 8, 1 bRG cell leads on average to the generation of 5,75 bRG cells, 1,21 IPs and 2,69 neurons, highlighting their strong self-amplification potential (Fig. 3f). Modeling bRG output through time reveals that bRG amplification increases from stage 7 to 9 and decreased from 13 to 15 (Fig 3g). Strikingly, this occurs at a relatively constant neurogenic rate indicating that, at the single progenitor level, self-amplification varies but not the number of differentiated cells produced. Finally, we tested how variations in cell fate decision probabilities would affect their output. Reducing the rate of proliferative divisions by 20% in favor of asymmetric self-renewing indirect divisions (1bRG + 1 IP) - the dominant division mode in mouse aRG cells at neurogenesis onset – reduced the total production of bRG cells by 31% after only 4 divisions (Extended data Fig. 4b). Overall, this analysis indicates that bRG cells are highly proliferative and undergo important self-amplification. Upon differentiation, they undergo frequent self-consuming terminal divisions, as well as abundant direct neurogenesis.

A map of cell fate decisions in human fetal tissue

We next adapted this correlative imaging method to human frontal cortex samples at GW 14-18. While slices were substantially larger, the macro proved to be very efficient at automatically identifying and aligning corresponding regions between the live and fixed datasets, indicating that it can be used for any type of tissues (Fig. 4a, b). We analyzed the division modes of 227 human fetal bRG cells, following 48-hour live imaging (Fig. 4c, extended data Fig. 5a and Supplementary Video; 9, 10). We confirmed the rapid expression of differentiation markers following cell division (Extended Data Fig. 5b). As in cerebral organoids, the majority of bRG cells performed symmetric proliferative division, generating two SOX2+ daughters (Fig. 4d, e). At GW18, we noted a decrease in neurogenic division in favor of gliogenic divisions, indicating that the switch begins around this developmental time. Within neurogenic divisions, we again observed abundant symmetric self-consuming divisions that remained relatively constant (around 32% of all neurogenic divisions) (Fig. 4d, f). Finally, we confirmed that direct neurogenic divisions are an abundant bRG cell division mode, which again remained stable from GW14 to 18 (over 40% of all neurogenic divisions) (Fig. 4d, g). We tested whether these cell fate decisions varied depending on bRG cell mitotic behaviors (apical MST, basal MST or static division) but found no clear effect of this parameter (Extended

Data Fig. 5c). Overall, we find a strong conservation of division modes between human fetal tissue and cerebral organoids, with the coexistence of asymmetric self-renewing progenitors – as classically observed in mouse aRG cells – together with self-amplifying and self-consuming neurogenic progenitors which represent an alternative route for neuronal generation.

Increased direct neurogenesis in the basal part of the human fetal OSVZ

The human OSVZ is extremely large (approximately 3 mm at GW17) and bRG cells may therefore be exposed to different microenvironments depending on their position, which may influence their division modes. Moreover, bRG cells progressively migrate through the SVZ and have a different history depending on their position. We therefore explored whether bRG division modes vary along the apico-basal axis in the human fetal brain. To test this, we adapted the above-described macro to automatically record the position of each dividing bRG cell within the tissue. Distance to the apical surface was measured at the time of cytokinesis. We then plotted the different division modes depending on bRG cell position within the tissue.

The position of bRG cells along the apico-basal axis only had a very minor effect on symmetric proliferative versus neurogenic division (Fig. 5a, b). Similarly, the rate of symmetric self-consuming versus asymmetric self-renewing divisions was not significantly different (Fig. 5a, b). However, we observed a clear difference in the rates of direct versus indirect neurogenesis, depending on the position in the tissue. Indeed, indirect neurogenic divisions (EOMES+ cells) occurred on average 800 μm from the apical surface, while direct neurogenic divisions (NEUN+ cells) occurred much more basally, 1,306 μm from the apical surface (Fig. 5a, b). These experiments could not be performed in cerebral organoids, as they display a much smaller OSVZ. Overall, they demonstrate that dividing bRG cells undergo more direct neurogenic divisions when located in the basal part of the fetal OSVZ.

Basal process inheritance does not predict bRG fate upon asymmetric division

The mechanism of bRG cell asymmetric division remains unknown. In mouse aRG cells, growing evidence support the role of basal process inheritance in stem cell fate maintenance[30-32]. We therefore used our correlative imaging method to test whether process inheritance correlates with bRG fate maintenance upon asymmetric division of human bRG cells. We first live imaged 79 asymmetrically-dividing bRG cells (one bRG daughter – one differentiating daughter) within week 8-10 cerebral organoids, and analyzed daughter cell fate depending on process inheritance (Fig. 6a, b and Supplementary Videos 11, 12). In half of these cells, process-inheriting daughters maintained a bRG fate but in the other half, process-

inheriting daughters differentiated (Fig. 6c, d). This was the case whether the asymmetric divisions generated an IP or directly a neuron. These results suggest no role for process inheritance in bRG fate upon asymmetric cell division in cerebral organoids. We next performed a similar analysis in GW 14-17 human fetal brain tissue. We analyzed 82 asymmetrically dividing bRG cells and again found no correlation between basal process inheritance and bRG cell fate (Fig. 6e, f and Supplementary Videos 13, 14): 52.4% of basal process-inheriting daughters remained bRG cells, and 47.6% differentiated (Fig. 6g, h). We did not observe any effect of the apical process on cell fate either (not shown). In support of these results, SOX2+ daughter cells that did not inherit a process could be observed to regrow a novel basal process after division (Extended Data Fig. 6 and Supplementary Video 15). Therefore, in human bRG cells, the basal process appears to be a consequence, rather than a cause, of bRG cell fate upon asymmetric division. Its presence during interphase may however participate in long-term bRG fate maintenance.

Notch signaling is active in bRG daughters, not in process-inheriting cells

We next addressed why basal process inheritance correlates with stem cell fate in mouse aRG cells but not in human bRG cells, using the cerebral organoid model. In aRG cells, it was proposed that the basal process acts as an antenna for the reception of Notch signaling from the surrounding cells, in particular neurons[31,32]., We first validated the role of Notch signaling for bRG cell self-renewal in cerebral organoids[4]. Following retroviral infection to deliver GFP, slices were treated with the γ-secretase inhibitor DAPT – which blocks Notch signaling – for 2 days. Quantification revealed a depletion of GFP+ bRG cells in favor of IPs, but not of neurons (Extended Data Fig 7a, b). Therefore, indirect neurogenesis is the default differentiation pathway in the absence of Notch signaling. We next investigated Notch signaling in bRG daughter cells, depending on process inheritance. As a readout, we analyzed the expression of its downstream target HES1. In cerebral organoids, HES1 was strongly expressed in the VZ where aRG cells are highly abundant and in a sparse manner in the SVZ, reflecting the SOX2+ bRG cell distribution (Fig. 7a). Week 8-11 organoid slices were live imaged for 48 hours, stained for HES1, EOMES and NEUN, and processed through the correlative imaging protocol. Cell fate was determined based on EOMES and NEUN expression, with double-negative cells being identified as bRG cells. Out of 276 bRG cell, 186 performed symmetric proliferative divisions, 53 asymmetric divisions, and 37 symmetric self-consuming divisions (Fig. 7b). Consistent with its oscillatory behavior in RG cells[33], HES1 was only detected in a subset of bRG cells, whether these cells were generated following symmetric or asymmetric divisions

(Fig. 7c, d and Supplementary Video 16). As expected, HES1 was never detected in differentiating cells (n=90 cells) (Fig. 7d). In total, out of 276 live imaged bRG cells, we identified 16 cells that divided asymmetrically, with detectable HES1 expression in daughter cells (Fig. 7d). HES1 was always detected in the non-differentiating daughter (EOMES- and NEUN-), supporting preferential Notch signaling in the self-renewing bRG daughter upon asymmetric division (Fig. 7d). However, we found no correlation between HES1 expression and process inheritance: 8 HES1-expressing cells inherited the basal process and 8 did not (Fig. 7e, f and Supplementary Video 17). These data further support that process inheritance does not correlate with bRG cell fate, and that the basal process is not involved in differential Notch signaling upon asymmetric division in bRG cells, as it is believed to be in aRG cells.

Discussion

bRG cells are key actors in the evolutionary expansion of the human brain, but the sequence of events leading to their massive neuronal output is unknown. Using live/fixed correlative imaging, we provide a map of their division modes at early – mostly pre-gliogenic – stages. Identifying the precise cell fate decisions that lead to given neuronal outputs is critical to understand the diversity of differentiation trajectories taken by bRG cells. In mice, aRG cells undergo a precise switch in division modes at E12.5, from mostly symmetric amplifying divisions to mostly asymmetric divisions generating one self-renewing aRG cell and one IP that will divide once to generate two neurons[34-36]. Here we show that, at neurogenesis onset, multiple bRG cell division modes co-exist, pointing to a more complex regulation in the human cortex.

We observe that bRG amplification through symmetric cell divisions is dominant, and in organoids increases from weeks 7 to 9 and decreases from 13 to 15. Modelling reveals that this occurs at a constant rate of neurogenesis, indicating that, at each developmental stage, single bRG cells produce an equal number of differentiated cells, irrespective of their self-amplification level. At the population level however, the gradual increase in the total number of bRG cells during development will lead to an increase in the production of differenced cells. These results suggest that neuronal production increases through development as a consequence of the expanding pool of bRG cells, but not of increased neurogenic potential of single bRG cells.

Our results indicate that, on top of asymmetric self-renewing divisions, bRG cells undergo symmetric amplifying divisions and self-consuming divisions, pointing to an alternative route for neuronal generation. Neurogenic divisions are frequently direct, bypassing

IP production. This represents another major difference with mouse aRG cells that largely rely on IPs to amplify the neurogenic output. The evolution of cortical neurogenesis in amniotes is regulated by the balance between direct and indirect neurogenesis[37]. aRG cells in sauropsids undergo direct neurogenesis, while mammals largely rely on indirect divisions in the evolutionary more recent neocortex, a process associated with size expansion and regulated by Robo signaling levels[37]. We show that this rule does however not apply to bRG cells, in which direct neurogenesis is common. aRG cells rely on IPs to amplify their neurogenic output, and we hypostatize that this may occur because their own self-amplification is limited by spatial constraints. They must indeed divide at the ventricular surface to precisely segregate their apical junctions between daughters and maintain a proper neuroepithelial structure. Interkinetic Nuclear Migration (INM) leads to the formation of a pseudostratified epithelium that allows an increase in the aRG cell pool, but their amplification still reaches a physical limit[38-40]. bRG cells on the other hand are not subject to this physical limitation and can amplify their own pool both radially and tangentially. In this regard, IPs may be less relied upon to increase the neurogenic output. Whether direct and indirect divisions ultimately lead to the formation of different neuronal subtypes, as observed in aRG cells, remains to be tested[37].

Cerebral organoids have emerged as a powerful system to investigate human brain development[41-43]. To what degree they faithfully recapitulate fetal neurogenesis is however important to monitor. Genomics studies have highlighted the similarity of transcriptional profiles, though substantial metabolic stress has been reported in organoids[18-23]. Here, we report a high similarity of bRG cell division modes between organoids and fetal tissue. We note that direct neurogenesis is slightly more abundant in organoids, which may reflect cell stage differences or inherent limitations of the organoid model. Nevertheless, an advantage of imaging approaches such as ours is that the organoid necrotic core (from where most stress likely originates) can be avoided, focusing on the cortical-like lobes at the periphery of the organoids. These cortical-like structures are however much thinner than in the fetal brain, limiting the ability to probe how bRG cell position impacts their division modes, as performed here in fetal tissue.

The molecular mechanism regulating asymmetrical division in RG cells has been a matter of controversy. In aRG cells, increasing evidence support a role for the basal process in cell fate, which correlates with Notch activation and self-renewal[30-32]. We however do not observe such a correlation in human bRG cells where Notch signaling is activated in the self-renewing daughter irrespective of basal process inheritance. aRG somas are located in the ventricular zone and their basal process extends through the cortex, contacting neurons from

which Notch-Delta signaling can be activated. bRG somas on the other hand are located in the SVZ and both their daughter cells are in close proximity to neurons. Therefore, due to the bRG cell microenvironment, it is consistent that their basal process does not confer differential Notch signaling. Other factors, such as centriole age, mitochondrial dynamics, mitotic spindle positioning or Sara endosomes are promising candidates[44-46].

Descriptions of clonal relationships are a powerful means to understand cellular diversity. Key to this is the identification of the cell fate decision branch points along lineages. The semi-automated correlative imaging method enables to quantitatively measure progenitor cell division modes in human cortical tissue. This will allow to probe neuronal subtype generation or the switch to gliogenesis, through time and space, across species, and in pathological contexts.

Material and methods

Ethics statement:

Human fetal tissue samples were collected with previous patient consent and in strict observance of legal and institutional ethical regulations. The protocol was approved by the French biomedical agency (Agence de la Biomédecine, approval number: PFS17-003).

Data and code availability

The live imaging and immunofluorescence data that support the findings of this study are available from the corresponding author (alexandre.baffet@curie.fr) or from the first authors (coquand.laure@gmail.com - clarisse.brunet@curie.fr) upon request. The LiveFixedCorrelative code is available at **http://xfer.curie.fr/get/lhGgGtXKbHF/Codes_correlative.zip**

Human iPSC culture

The feeder-independent iPS cell line used for this study was a gift from Silvia Cappello (Max-Plank Institute of Psychiatry - Munich). Cells were reprogrammed from NuFF3-RQ human newborn foreskin feeder fibroblasts (GSC-3404, GlobalStel)[47]. iPS cells were cultivated as colonies on vitronectin-coated B3 dishes, using mTser medium (STEMCELL Technologies). Colonies were cleaned daily under a binocular stereo microscope (Lynx EVO, Vision Engineering), by manually removing differentiated cells with a needle.

Cerebral organoids culture

Cerebral organoids were derived from human iPS cells, following a previously published protocol [42]. Day 0 to day 4: iPS colonies of 1-2 mm of diameter were detached with pre-warmed collagenase (1mg/mL) for 45 min at 37°C. After the addition of 1 mL of mTser, floating colonies were transferred with a cut tip into a 15 ml tube for two series of gentle washing with medium 1 (DMEM-F12 without phenol red, 20% KOSR, 1X GlutaMAX, 1X MEM-NEAA, 1X 2-Mercaptoethanol, Pen/Strep, 2µM Dorsomorphin, 2 µM A-83). Colonies were subsequently distributed in an ultra-low attachment 6-well plate with 3 mL of medium 1 and cultivated at 37°C, 5% CO2. Day 5-6: Half of medium 1 was replaced daily with medium 2 (DMEM-F12 without phenol red, 1X N2 supplement, 1X GlutaMAX, 1X MEM-NEAA, Pen/Strep, 1 µM CHIR-99021, 1 µM SB-421542). Day 7-14: At day 7, EBs were embedded in Matrigel diluted in medium 2 at a ratio of 2:1. Matrigel-EB mixture was then spread in an ultra-low attachment dish and incubated at 37°C for 30 min to solidify (10-20 EBs per well). Finally, medium 2 was gently added to the well, without disturbing the Matrigel patch. On day 14, Matrigel was mechanically broken by pipetting with a 5 mL pipet and transferred into a 15 mL tube for gentle washing. Organoids were suspended in medium 3 (DMEM-F12 without phenol red, 1X N2 supplement, 1X b27 supplement, 1X GlutaMAX, 1X MEM-NEAA, 1X 2-Mercaptoethanol, Pen/Strep, 2.5 µg/mL Insulin) and grown in ultra-low attachment 6-well plates under agitation at 100 rpm (Digital Orbital Shaker DOS-10M from ELMI). Day 35 to 84: Starting from day 35, medium 3 was supplemented with diluted Matrigel (1:100) [48].

Infection of human fetal cortex and cerebral organoids

Fresh tissue from human fetal cortex was obtained from autopsies performed at the Robert Debré Hospital, and Necker enfants malades Hospital (Paris). Tissues came from spontaneous miscarriages or pregnancy terminations due to kidney malformations. or A piece of pre-frontal cortex was collected from one hemisphere, and transported on ice from the hospital to the lab. The tissue was divided into smaller pieces and embedded 4% low-gelling agarose (Sigma) dissolved in artificial cerebrospinal fluid (ACSF). Cerebral organoids (week 8-12) were embedded in 3% low-gelling agarose. Gel blocks from both tissues were then sliced with a Leica VT1200S vibratome (300 µm-thick slices) in ice-cold ACSF. Slices were infected with a GFP coding retrovirus, diluted in DMEM-F12. After 2h of incubation, slices were washed three times with DMEM-F12 and grown on Millicell cell culture inserts (Merck) in cortical culture medium (DMEM-F12 containing B27, N2, 10 ng/ml FGF, 10 ng/ml EGF, 5% fetal

bovine serum and 5% horse serum) for up to 5 days for human fetal brain and 48h for cerebral organoids. Medium was changed every day.

Live imaging in cerebral organoids and human fetal cortex slices

To follow bRG cell divisions for approximately 48h, we used the following approach. 48h after infection (3-5 days for human fetal brain), slices were placed under the microscope by transferring the culture inserts in a 35 mm FluoroDish (WPI) with 1 mL of culture medium (DMEM-F12 containing B27, N2, 10 ng/ml FGF, 10 ng/ml EGF, 5% fetal bovine serum and 5% horse serum). Live imaging was performed on a spinning disk wide microscope equipped with a Yokogawa CSU-W1 scanner unit to increase the field of view and improve the resolution deep in the sample. The microscope was equipped with a high working distance (WD 6.9-8.2 mm) 20X Plan Fluor ELWD NA 0.45 dry objective (Nikon), and a Prime95B SCMOS camera. Z-stacks of 80-100 µm range were taken with an interval of 4-5 µm, and maximum projections were performed. Videos were mounted in Metamorph. Image treatments (maximum projections, subtract background, Median filter, stackreg and rotation) were carried out on Fiji. Figures were assembled with Affinity Designer.

Immunostaining of brain slices

Human fetal brain and cerebral organoid slices in culture were fixed in 4% PFA for 2 hours. Slices were boiled in sodium citrate buffer (10 mM, pH 6) for 20 minutes and cooled down at room temperature (antigen retrieval). Slices were then blocked in PBS-Triton 100X 0.3%-donkey serum 2% at room temperature for 2 hours, incubated with primary antibody overnight at 4°C in blocking solution, washed in PBS-Tween 0.05%, and incubated with secondary antibody overnight at 4°C in blocking solution before final wash and mounting in Aquapolymount. Mosaics (tile scans) of fixed tissue were acquired with a CFI Apo LWD Lambda S 40X objective (WI NA 1.15 WD 0.61-0.59, Nikon).

Live and fixed correlative microscopy analysis

The correlative microscopy method enables to automatically pair and align live and fixed samples, for cell-cell matching. The macro, based on ImageJ [49] and Matlab, enables automated contouring of the slices, matching of the live and fixed samples based on their area and shape, and alignment of the samples (rotation and flip if needed). This leads to the precise positioning of the live imaged cells on the immunostained images. This method is described in detail in the **Annex 1**.

Mathematical model

The model considers 3 different cell types: bRG cells are type A, IP are type B, and neurons are type C. The number of each cell type after *x* division is written I_x (with I=A, B, C) and the probability of producing a cell of type *I* and a cell of type *J* after a bRG division is written p_{ij}, The average number of the different cell type after x division satisfies the recurrence relations:

$$A_x = A_{x-1}(2p_{aa} + p_{ab} + p_{ac}), B_x = B_{x-1} + A_{x-1}(p_{ab} + 2p_{bb}), C_x = C_{x-1} + A_{x-1}(p_{ac} + 2p_{cc})$$

Therefore, after x division, the average number of cells of each cell type are

$$A_x = A_0\overline{p_a}^x, B_x = A_0\overline{p_b}\frac{\overline{p_a}^x - 1}{\overline{p_a} - 1}, C_x = A_0\overline{p_c}\frac{\overline{p_a}^x - 1}{\overline{p_a} - 1},$$

with

$$\overline{p_a} = 2p_{aa} + p_{ab} + p_{ac}, \overline{p_b} = p_{ab} + 2p_{bb}, \overline{p_c} = p_{ac} + 2p_{cc}\ .$$

The number of bRG cells increases exponentially with the number of division if $\overline{p_a} > 1$ and decreases if $\overline{p_a} < 1$. In the former case, the ratio of non bRG to bRG cells reaches a constant value $\frac{IP+Neurons}{bRG} = \frac{2-\overline{p_a}}{\overline{p_a}-1}$.

Retrovirus production

To improve transfection efficiency, we used the HEK-Phoenix-GP cell line that stably expresses the packaging enzymes GAL and POL. Cells were plated in 3xT300 (dilution at 1:20) and grown for 3 days to reach 70% of confluence in DMEM-GlutaMax medium, 10% FBS (50 mL/flask). At day 3, cells were transfected with envelope VSVG plasmid and transfer plasmid (CAG-GFP or MSCV-IRES-GFP) using Lipofectamine 2000. The two plasmids were mixed into 5.4 mL of OptiMEM medium (18 µg E-plasmid / 49.5 µg t-plasmid). 337.5 µL of Lipofectamine 2000 was diluted in 5.4 mL of OptiMEM medium and incubated 5 min at room temperature. The DNA preparation was thoroughly mixed into the Lipofectamine preparation and incubated for 30 min at room temperature. In the meantime, medium was changed by 30 mL of DMEM-Glutamax (without FBS) per T300 flask. 3.6 mL of the DNA-Lipofectamine mixture was then added to each T300 flask and incubated for 5h in a 37°C incubator. After this period, flasks were carefully transferred into an L3 lab and the medium was changed for 30 mL of fresh DMEM-GlutaMAX, 10% FBS. At day 5, medium was harvested into 50 mL tubes and replaced by 30 mL of fresh medium (samples were stored at 4°C). At day 6, medium was harvested, pooled with Day 5 samples and spun-down to pellet cell debris (1300 rpm, 5 min at 4°C). Supernatant was then filtered using 0.22 µm filter unit and divided into 6 Ultra-Clear tubs

(Beckman Coulter – Ref.344058). Tubes were ultra-centrifuged at 31000 G for 1h30 at 4°C. Supernatant was removed, retroviruses were collected with multiple PBS washings and transferred into a single new Ultra-Clear tub. Final ultra-centrifugation was performed (31000 G for 1h30 at 4°C), supernatant was carefully removed and the thin pellet of retroviruses was suspended into 750 µL of DMEM-F12 medium, aliquoted (50 to 100 µL aliquots) and stored at -80°C. Titer of the preparation was tested by infecting regular HEK cells at different dilution and the percentage of GFP+ cells was measured by FACS.

NOTCH inhibition experiments

For Notch inhibition experiments, 250µm-thick organoid slices were infected with a GFP expressing retrovirus as described above. After infection, slices were transferred to Millicell cell culture inserts (Merck) and placed in a 6-well plate containing cortical culture medium supplemented with 5µM of DAPT (Tocris, 2364). Culture medium was refreshed every day. After 48 hours, organoid slices were fixed, and immunostaining was performed. Cortical culture medium was supplemented with DMSO for the control condition.

Expression constructs and antibodies

The following plasmids were used in this study: CAG-GFP (a gift from Victor Borrell); MSCV-IRES-GFP (Tannishtha Reya, Addgene 20672); VSVG (a gift from Philippe Benaroch). Antibodies used in this study were mouse anti-SOX2 (Abcam Ab79351, 1/500), sheep anti-EOMES (R&D Sytems AF6166, 1/500), rabbit anti-NEUN (Abcam Ab177487, 1/500), chicken anti-GFP (Abcam Ab13970, 1/500), mouse anti-pVimentin (Abcam Ab22651, 1/1000), rat anti-HES1 (MBL D134-3, 1/500), rabbit anti-NeuroD2 (Abcam, ab104430, 1/500), mouse anti-HuC/HuD (ThermoFisher Scientific, A-21271, 1/200), rabbit anti-HOPX (Proteintech, 11419-1-AP, 1/500), mouse anti-S100β (Synaptic systems 287111, 1/500), mouse anti-OLIG2 (Millipore MABN50, 1/200).

Acknowledgements

We acknowledge Institut Curie, member of the French National Research Infrastructure France-BioImaging (ANR10-INBS-04) and the Nikon BioImaging Center (Institut Curie, France). We thank Fiona Francis (IFRM) and Xavier Morin for helpful discussions and critical reading of the manuscript. L.C. was funded by the French ministry of research (MESRI). A-S.M. was funded by the Labex Cell(n)Scale and CNRS. A.D.B. is an INSERM researcher**.** This work was

supported by the CNRS, I. Curie, the ANR (ANR-20-CE16-0004-01) and the Ville de Paris "Emergences" program.

Author contributions

L.C. and C.B.A performed experiments, analyzed data and wrote the manuscript. A-S.M. coded the LiveFixedCorrelative macro, S.F., A.D.C. and M.L. generated organoids, B.S, T.A-B. and F.G. provided fetal tissue, V.F. assisted with imaging, P. S. generated the mathematical model, J-B. B. designed the project, performed experiments and analyzed data, and A.D.B. designed the project and wrote the manuscript.

References

1. Cadwell, C. R., Bhaduri, A., Mostajo-Radji, M. A., Keefe, M. G. & Nowakowski, T. J. Development and Arealization of the Cerebral Cortex. *Neuron* **103,** 980–1004 (2019).
2. Nowakowski, T. J., Pollen, A. A., Sandoval-Espinosa, C. & Kriegstein, A. R. Transformation of the Radial Glia Scaffold Demarcates Two Stages of Human Cerebral Cortex Development. *Neuron* **91,** 1219–1227 (2016).
3. Smart, I. H. M., Dehay, C., Giroud, P., Berland, M. & Kennedy, H. Unique morphological features of the proliferative zones and postmitotic compartments of the neural epithelium giving rise to striate and extrastriate cortex in the monkey. *Cereb. Cortex* **12,** 37–53 (2002).
4. Hansen, D. V., Lui, J. H., Parker, P. R. L. & Kriegstein, A. R. Neurogenic radial glia in the outer subventricular zone of human neocortex. *Nature* **464,** 554–561 (2010).
5. Fietz, S. A. *et al.* OSVZ progenitors of human and ferret neocortex are epithelial-like and expand by integrin signaling. *Nat Neurosci* **13,** 690–699 (2010).
6. Reillo, I., De Juan Romero, C., García-Cabezas, M. Á. & Borrell, V. A role for intermediate radial glia in the tangential expansion of the mammalian cerebral cortex. *Cerebral Cortex* **21,** 1674–1694 (2011).
7. Wang, X., Tsai, J.-W., LaMonica, B. & Kriegstein, A. R. A new subtype of progenitor cell in the mouse embryonic neocortex. *Nat Neurosci* **14,** 555–561 (2011).
8. Vaid, S. *et al.* A novel population of Hopx-dependent basal radial glial cells in the developing mouse neocortex. *Development* **145,** dev169276–39 (2018).
9. Dehay, C., Kennedy, H. & Kosik, K. S. The outer subventricular zone and primate-specific cortical complexification. *Neuron* **85,** 683–694 (2015).
10. LaMonica, B. E., Lui, J. H., Hansen, D. V. & Kriegstein, A. R. Mitotic spindle orientation predicts outer radial glial cell generation in human neocortex. *Nature Communications* **4,** 1665–11 (2013).
11. Martínez-Martínez, M. Á. *et al.* A restricted period for formation of outer subventricular zone defined by Cdh1 and Trnp1 levels. *Nature Communications* **7,** 11812 (2016).
12. Betizeau, M. *et al.* Precursor diversity and complexity of lineage relationships in the outer subventricular zone of the primate. *Neuron* **80,** 442–457 (2013).
13. Ostrem, B. E. L., Lui, J. H., Gertz, C. C. & Kriegstein, A. R. Control of outer radial glial stem cell mitosis in the human brain. *CellReports* **8,** 656–664 (2014).

14. Fernández, V., Llinares-Benadero, C. & Borrell, V. Cerebral cortex expansion and folding: what have we learned? *EMBO J* (2016). doi:10.15252/embj.201593701
15. Pollen, A. A. *et al.* Molecular identity of human outer radial glia during cortical development. *Cell* **163,** 55–67 (2015).
16. Florio, M. *et al.* Human-specific gene ARHGAP11B promotes basal progenitor amplification and neocortex expansion. *Science* **347,** 1465–1470 (2015).
17. Nowakowski, T. J. *et al.* Spatiotemporal gene expression trajectories reveal developmental hierarchies of the human cortex. *Science* **358,** 1318–1323 (2017).
18. Pollen, A. A. *et al.* Establishing Cerebral Organoids as Models of Human-Specific Brain Evolution. *Cell* **176,** 743–756.e17 (2019).
19. Bhaduri, A. *et al.* Cell stress in cortical organoids impairs molecular subtype specification. *Nature* **578,** 142–148 (2020).
20. Velasco, S. *et al.* Individual brain organoids reproducibly form cell diversity of the human cerebral cortex. *Nature* **570,** 523–527 (2019).
21. Camp, J. G. *et al.* Human cerebral organoids recapitulate gene expression programs of fetal neocortex development. *Proc Natl Acad Sci USA* **112,** 15672–15677 (2015).
22. Amiri, A. *et al.* Transcriptome and epigenome landscape of human cortical development modeled in organoids. *Science* **362,** (2018).
23. Kanton, S. *et al.* Organoid single-cell genomic atlas uncovers human-specific features of brain development. *Nature* **574,** 418–422 (2019).
24. Lui, J. H. *et al.* Radial glia require PDGFD-PDGFRβ signalling in human but not mouse neocortex. *Nature* **515,** 264–268 (2014).
25. Fiddes, I. T. *et al.* Human-Specific NOTCH2NL Genes Affect Notch Signaling and Cortical Neurogenesis. *Cell* **173,** 1356–1369.e22 (2018).
26. Suzuki, I. K. *et al.* Human-Specific NOTCH2NL Genes Expand Cortical Neurogenesis through Delta/Notch Regulation. *Cell* **173,** 1370–1384.e16 (2018).
27. Gao, P. *et al.* Deterministic progenitor behavior and unitary production of neurons in the neocortex. *Cell* **159,** 775–788 (2014).
28. He, Z. *et al.* Lineage recording in human cerebral organoids. *Nature methods* 1–10 (2021). doi:10.1038/s41592-021-01344-8
29. Fischer, E. & Morin, X. Fate restrictions in embryonic neural progenitors. *Current Opinion in Neurobiology* **66,** 178–185 (2021).
30. Alexandre, P., Reugels, A. M., Barker, D., Blanc, E. & Clarke, J. D. W. Neurons derive from the more apical daughter in asymmetric divisions in the zebrafish neural tube. *Nat Neurosci* **13,** 673–679 (2010).
31. Shitamukai, A., Konno, D. & Matsuzaki, F. Oblique radial glial divisions in the developing mouse neocortex induce self-renewing progenitors outside the germinal zone that resemble primate outer subventricular zone progenitors. *Journal of Neuroscience* **31,** 3683–3695 (2011).
32. Peyre, E. & Morin, X. An oblique view on the role of spindle orientation in vertebrate neurogenesis. *Develop. Growth Differ.* **54,** 287–305 (2012).
33. Ochi, S., Imaizumi, Y., Shimojo, H., Miyachi, H. & Kageyama, R. Oscillatory expression of Hes1 regulates cell proliferation and neuronal differentiation in the embryonic brain. *Development* **147,** (2020).
34. Noctor, S. C., Martínez-Cerdeño, V., Ivic, L. & Kriegstein, A. R. Cortical neurons arise in symmetric and asymmetric division zones and migrate through specific phases. *Nat Neurosci* **7,** 136–144 (2004).
35. Haubensak, W., Attardo, A., Denk, W. & Huttner, W. B. Neurons arise in the basal neuroepithelium of the early mammalian telencephalon: a major site of neurogenesis. *Proc Natl Acad Sci USA* **101,** 3196–3201 (2004).

36. Miyata, T. *et al.* Asymmetric production of surface-dividing and non-surface-dividing cortical progenitor cells. **131,** 3133–3145 (2004).
37. Huilgol, A. *et al.* Direct and indirect neurogenesis generate a mosaic of distinct glutamatergic projection neuron in cerebral cortex. *Neuron* **111,** 2557-2569.e4 (2023).
38. Hu, D. J.-K. *et al.* Dynein recruitment to nuclear pores activates apical nuclear migration and mitotic entry in brain progenitor cells. *Cell* **154,** 1300–1313 (2013).
39. Lee, H. O. & Norden, C. Mechanisms controlling arrangements and movements of nuclei in pseudostratified epithelia. *Trends Cell Biol* **23,** 141–150 (2013).
40. Baffet, A. D., Hu, D. J. & Vallee, R. B. Cdk1 Activates Pre-mitotic Nuclear Envelope Dynein Recruitment and Apical Nuclear Migration in Neural Stem Cells. *Dev Cell* **33,** 703–716 (2015).
41. Lancaster, M. A. *et al.* Cerebral organoids model human brain development and microcephaly. *Nature* **501,** 373–379 (2013).
42. Qian, X. *et al.* Brain-Region-Specific Organoids Using Mini-bioreactors for Modeling ZIKV Exposure. *Cell* **165,** 1238–1254 (2016).
43. Paşca, A. M. *et al.* Functional cortical neurons and astrocytes from human pluripotent stem cells in 3D culture. *Nature methods* **12,** 671–678 (2015).
44. Wang, X. *et al.* Asymmetric centrosome inheritance maintains neural progenitors in the neocortex. *Nature* **461,** 947–955 (2009).
45. Iwata, R., Casimir, P. & Vanderhaeghen, P. Mitochondrial dynamics in postmitotic cells regulate neurogenesis. *Science* **369,** 858–862 (2020).
46. Kressmann, S., Campos, C., Castanon, I., Fürthauer, M. & González-Gaitán, M. Directional Notch trafficking in Sara endosomes during asymmetric cell division in the spinal cord. *Nat Cell Biol* **17,** 333–339 (2015).
47. Kyrousi, C. *et al.* Extracellular LGALS3BP regulates neural progenitor position and relates to human cortical complexity. *Nature Communications* **12,** 6298–22 (2021).
48. Giandomenico, S. L. *et al.* Cerebral organoids at the air-liquid interface generate diverse nerve tracts with functional output. *Nat Neurosci* **22,** 669–679 (2019).
49. Schindelin, J. *et al.* Fiji: an open-source platform for biological-image analysis. *Nature methods* **9,** 676–682 (2012).

Figure 1

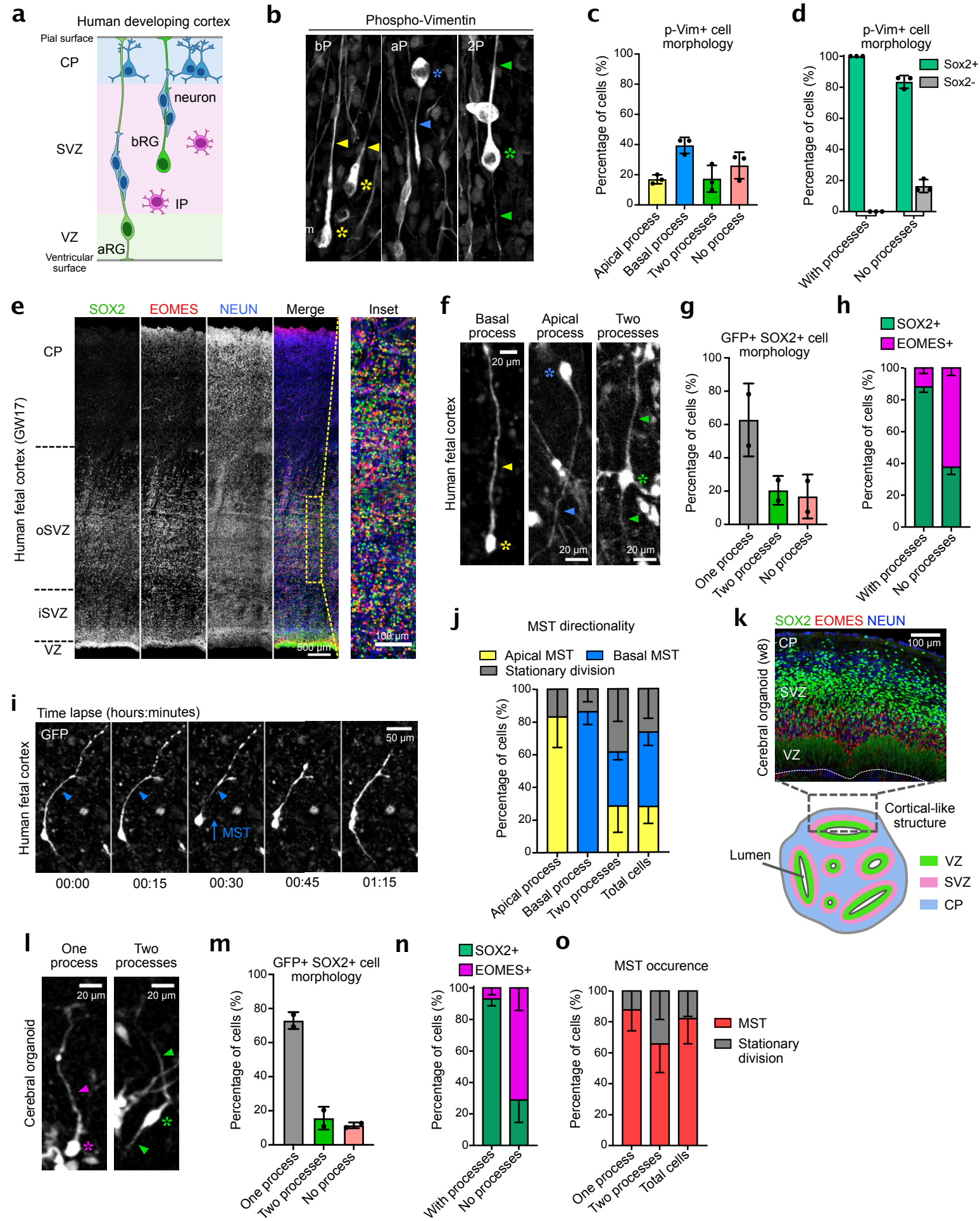
a
Human developing cortex
Pial surface
CP
neuron
SVZ
bRG
IP
VZ
aRG
Ventricular surface
b
Phospho-Vimentin
bP
aP
2P
c
p-Vim+ cell morphology
Percentage of cells (%)
Apical process
Basal process
Two processes
No process
d
p-Vim+ cell morphology
Sox2+
Sox2-
With processes
No processes
e
SOX2
EOMES
NEUN
Merge
Inset
Human fetal cortex (GW17)
CP
oSVZ
iSVZ
VZ
500 µm
100 µm
f
Basal process
Apical process
Two processes
Human fetal cortex
20 µm
g
GFP+ SOX2+ cell morphology
One process
Two processes
No process
h
SOX2+
EOMES+
With processes
No processes
i
Time lapse (hours:minutes)
GFP
Human fetal cortex
MST
50 µm
00:00
00:15
00:30
00:45
01:15
j
MST directionality
Apical MST
Basal MST
Stationary division
Total cells
k
SOX2 EOMES NEUN
Cerebral organoid (w8)
CP
SVZ
VZ
100 µm
Cortical-like structure
Lumen
l
One process
Two processes
Cerebral organoid
20 µm
m
GFP+ SOX2+ cell morphology
n
SOX2+
EOMES+
With processes
No processes
o
MST occurence
MST
Stationary division
Total cells

Fig. 1 Morphological characterization of bRG cells in human cerebral organoids and fetal tissue. a, Schematic representation of human neocortex development. VZ: ventricular zone. SVZ: subventricular zone. CP: cortical plate. aRG: apical radial glial progenitor. bRG: basal radial glial progenitor. IP: Intermediate progenitor. **b,** Phospho-Vimentin immunostaining of human frontal cortex at GW18. Image is overexposed to visualize processes, revealing cells with basal process (bP), apical process (aP) and two processes (2P). Asterix indicate soma and arrowheads indicate processes. **c,** Quantification of mitotic bRG cell morphologies in GW 14-18 frontal cortex. (N=3 brains, 338 cells). **d,** Percentage of p-VIM+ cells positive for SOX2, depending on morphology. (N=3 brains, 456 cells). **e,** SOX2, EOMES and NEUN immunostaining in human frontal cortex at GW17. **f,** Morphologies of GFP-expressing SOX2+ cells in human frontal cortex at GW17. **g,** Quantification of morphologies of GFP expressing SOX2+ cells in human frontal cortex at GW 14-17 (N=2 brains, 350 cells). **h,** Percentage of SOX2+/EOMES- and EOMES+ (with or without SOX2) progenitors, depending on morphology in human frontal cortex at GW 14-17 (N=2 brains, 204 cells). **i,** Live imaging of bRG cell performing MST in human fetal tissue. Arrowhead indicates basal process. **j,** Directionality of MST depending on bRG cell morphology in human frontal cortex at GW 14-18 (N=3 brains, 242 cells). **k,** (Top) SOX2, EOMES and NEUN immunostaining in week 8 cerebral organoid. (Bottom) Schematic representation of week 8-10 cerebral organoids. **l,** Morphologies of GFP expressing SOX2+ cells in cerebral organoids at weeks 7-10. **m,** Quantification of morphologies of GFP-expressing SOX2+ cells in cerebral organoids at weeks 7-8. (N=2 batches, 104 cells) **n,** Percentage of SOX2+/EOMES- and EOMES+ (with or without SOX2) progenitors, depending on morphology in cerebral organoids at weeks 8-10. (N=3 batches, 205 cells) **o,** Directionality of MST depending on bRG cell morphology cerebral organoids at weeks 8-9 (N=4 batches, 260 cells). Error bars indicate SD.

Figure 2

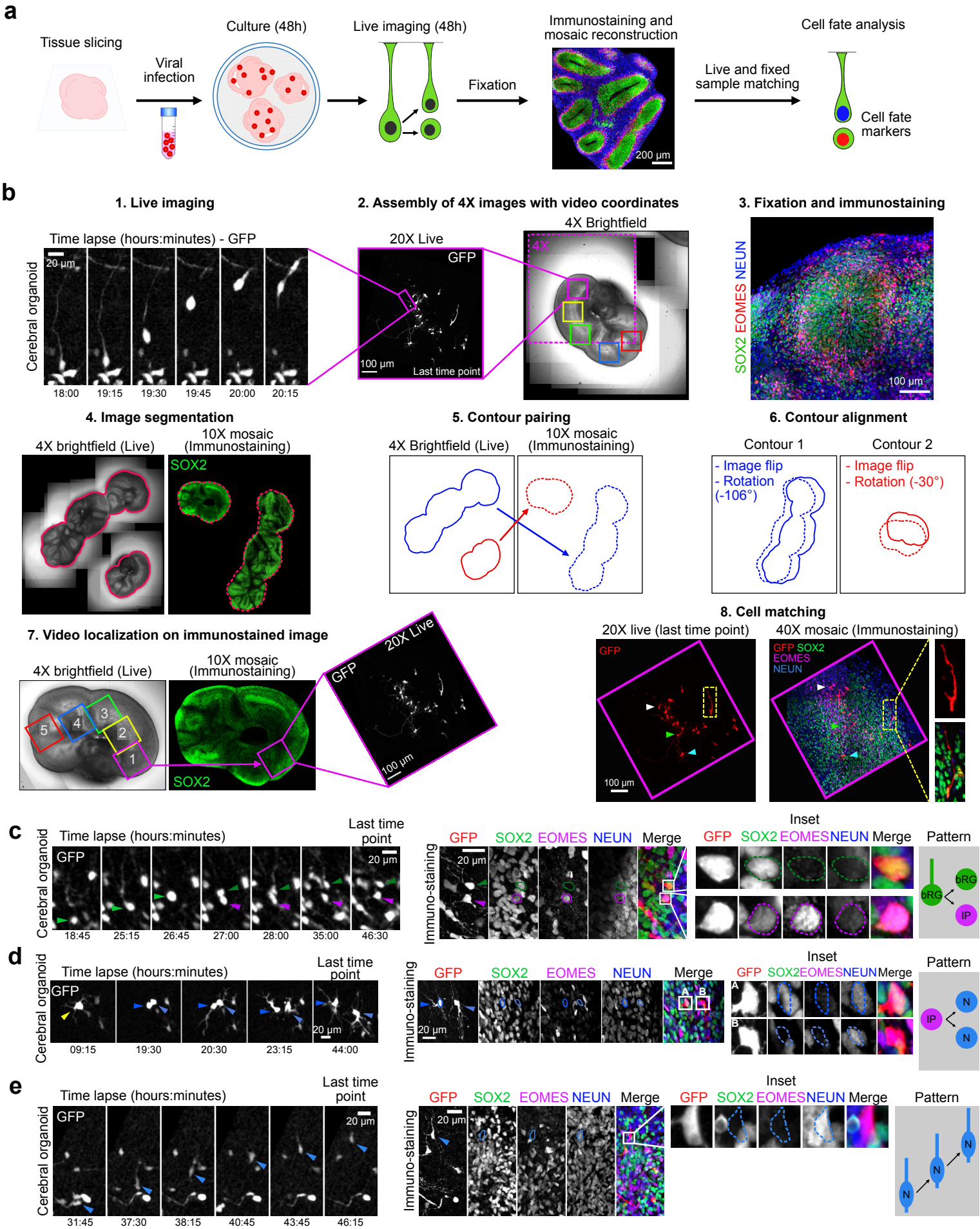
a
Tissue slicing
Viral infection
Culture (48h)
Live imaging (48h)
Fixation
Immunostaining and mosaic reconstruction
200 µm
Live and fixed sample matching
Cell fate analysis
Cell fate markers
b
1. Live imaging
Time lapse (hours:minutes) - GFP
Cerebral organoid
20 µm
18:00
19:15
19:30
19:45
20:00
20:15
2. Assembly of 4X images with video coordinates
20X Live
GFP
100 µm
Last time point
4X Brightfield
4X
3. Fixation and immunostaining
SOX2 EOMES NEUN
100 µm
4. Image segmentation
4X brightfield (Live)
10X mosaic (Immunostaining)
SOX2
5. Contour pairing
4X Brightfield (Live)
10X mosaic (Immunostaining)
6. Contour alignment
Contour 1
Contour 2
- Image flip
- Rotation (-106°)
- Image flip
- Rotation (-30°)
7. Video localization on immunostained image
4X brightfield (Live)
10X mosaic (Immunostaining)
1
2
3
4
5
SOX2
20X Live
GFP
100 µm
8. Cell matching
20X live (last time point)
40X mosaic (Immunostaining)
GFP
100 µm
GFP SOX2
EOMES
NEUN
c
Time lapse (hours:minutes)
Last time point
Cerebral organoid
GFP
20 µm
18:45
25:15
26:45
27:00
28:00
35:00
46:30
Immuno-staining
GFP SOX2 EOMES NEUN Merge
Inset
GFP SOX2 EOMES NEUN Merge
Pattern
bRG
IP
d
Time lapse (hours:minutes)
Last time point
Cerebral organoid
GFP
20 µm
09:15
19:30
20:30
23:15
44:00
Immuno-staining
GFP SOX2 EOMES NEUN Merge
Inset
GFP SOX2 EOMES NEUN Merge
Pattern
N
IP
N
e
Time lapse (hours:minutes)
Last time point
Cerebral organoid
GFP
20 µm
31:45
37:30
38:15
40:45
43:45
46:15
Immuno-staining
GFP SOX2 EOMES NEUN Merge
Inset
GFP SOX2 EOMES NEUN Merge
Pattern
N
N
N

Fig. 2 A semi-automated correlative imaging method to identify cell fate decisions in cerebral organoids.

a, Schematic representation of correlative microscopy pipeline. **b,** Step-by-step protocol for semi-automated correlative microscopy. (1) bRG cells are live imaged for 48 hours. (2) 4X brightfield images containing the video coordinates are assembled. (3) Organoid slices are fixed, immunostained for SOX2, EOMES and NEUN and imaged. (4) Images are automatically segmented to outline slices from live and fixed samples. (5) Slice contours are automatically paired based on shape and area and (6) aligned (including a horizontal flip if needed). (7) Video fields of view are automatically annotated on the immunostaining images. (8) Regions of interest are re-imaged at higher resolution 40X and cells from live and fixed samples are manually matched. **c,** Live/fixed correlative analysis of a dividing bRG cell generating a self-renewing bRG daughter and a differentiating IP daughter. **d,** Live/fixed correlative analysis of a dividing IP cell generating two neuronal daughters. **e,** Live/fixed correlative analysis of a migrating neuron.

Figure 3

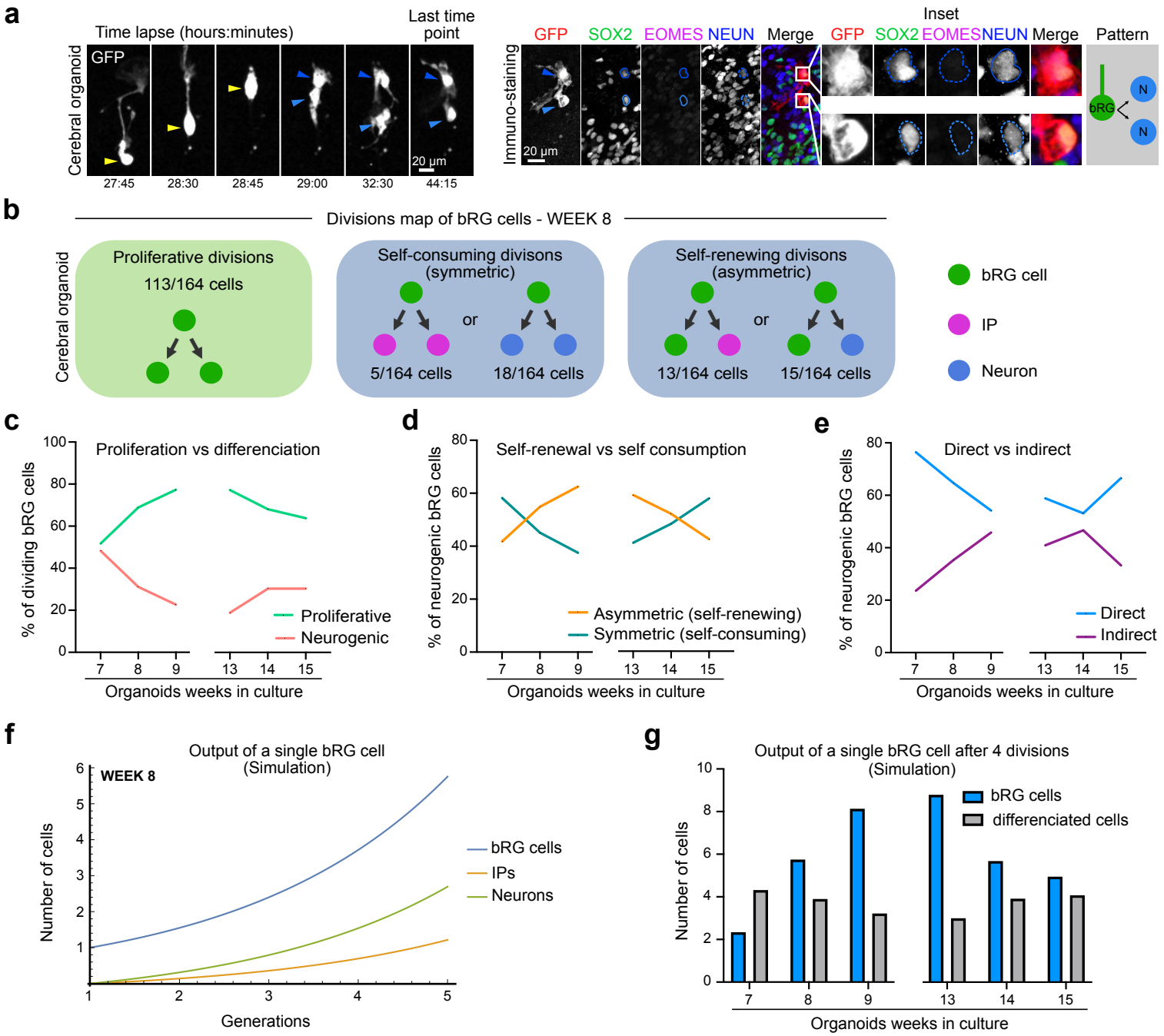
a
Time lapse (hours:minutes)
Last time point
Cerebral organoid
GFP
20 µm
27:45
28:30
28:45
29:00
32:30
44:15
Inset
GFP SOX2 EOMES NEUN Merge
GFP SOX2 EOMES NEUN Merge
Pattern
Immuno-staining
20 µm
bRG
N
N
b
Divisions map of bRG cells - WEEK 8
Cerebral organoid
Proliferative divisions
113/164 cells
Self-consuming divisons (symmetric)
or
5/164 cells
18/164 cells
Self-renewing divisons (asymmetric)
or
13/164 cells
15/164 cells
bRG cell
IP
Neuron
c
Proliferation vs differenciation
% of dividing bRG cells
Proliferative
Neurogenic
Organoids weeks in culture
d
Self-renewal vs self consumption
% of neurogenic bRG cells
Asymmetric (self-renewing)
Symmetric (self-consuming)
Organoids weeks in culture
e
Direct vs indirect
% of neurogenic bRG cells
Direct
Indirect
Organoids weeks in culture
f
Output of a single bRG cell (Simulation)
WEEK 8
Number of cells
bRG cells
IPs
Neurons
Generations
g
Output of a single bRG cell after 4 divisions (Simulation)
Number of cells
bRG cells
differenciated cells
Organoids weeks in culture

Fig. 3 A map of cell fate decisions in human cerebral organoids.

a, Live/fixed correlative analysis of a dividing bRG cell generating two neuronal daughters. **b,** Summary of all division patterns identified in bRG cells in week 8 cerebral organoids (N=164 bRG cells). **c,** Percentage of proliferative versus neurogenic divisions of bRG cells in week 7-9 and 13-15 cerebral organoids. **d,** Percentage of asymmetric (self-renewing) versus symmetric (self-consuming) neurogenic divisions of bRG cells in week 7-9 and 13-15 cerebral organoids. **e,** Percentage of direct versus indirect neurogenic divisions of bRG cells in week 7-9 and 13-15 cerebral organoids. Week 7 (N=114 bRG cells), week 8 (N=164 bRG cells), week 9 (N=106 bRG cells), week 13 (N=206 bRG cells), week 14 (N=254 bRG cells) and week 15 (N=257 bRG cells) (**c-e**). **f**, Simulation of the output of a single bRG cell after 1-5 generations, based on week 8 fate decision probabilities. **g**, Simulation of the output of a single bRG cell after 4 divisions (5 generations) in week 7-9 and 13-15 cerebral organoids.

Figure 4

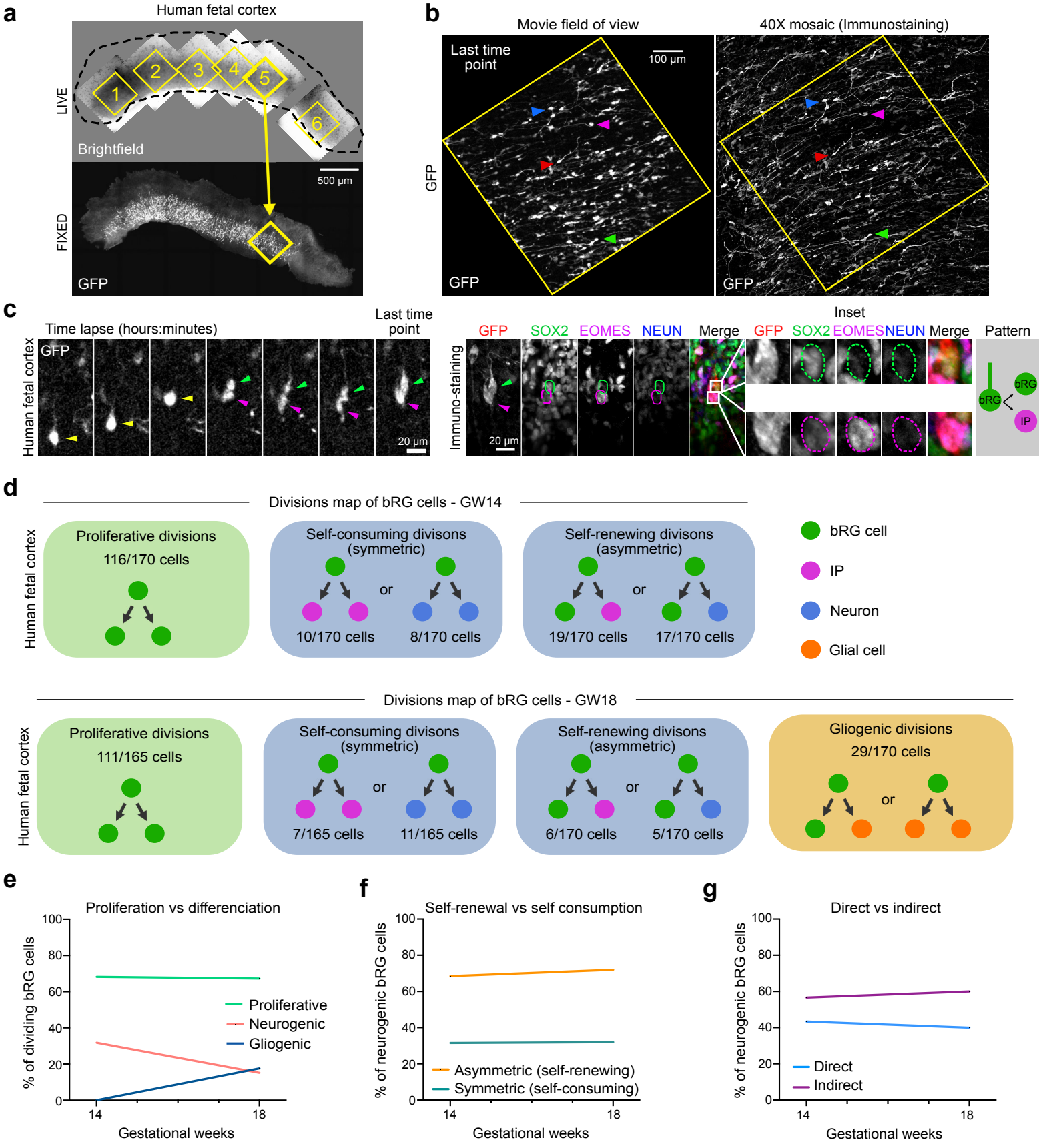
a
Human fetal cortex
LIVE
Brightfield
FIXED
GFP
500 µm
1
2
3
4
5
6
b
Movie field of view
40X mosaic (Immunostaining)
Last time point
100 µm
GFP
c
Time lapse (hours:minutes)
Last time point
Human fetal cortex
20 µm
Inset
GFP SOX2 EOMES NEUN Merge
Pattern
Immuno-staining
bRG
IP
d
Divisions map of bRG cells - GW14
Human fetal cortex
Proliferative divisions
116/170 cells
Self-consuming divisons (symmetric)
or
10/170 cells
8/170 cells
Self-renewing divisons (asymmetric)
19/170 cells
17/170 cells
bRG cell
IP
Neuron
Glial cell
Divisions map of bRG cells - GW18
Proliferative divisions
111/165 cells
7/165 cells
11/165 cells
6/170 cells
5/170 cells
Gliogenic divisions
29/170 cells
e
Proliferation vs differenciation
% of dividing bRG cells
Proliferative
Neurogenic
Gliogenic
Gestational weeks
f
Self-renewal vs self consumption
% of neurogenic bRG cells
Asymmetric (self-renewing)
Symmetric (self-consuming)
Gestational weeks
g
Direct vs indirect
% of neurogenic bRG cells
Direct
Indirect
Gestational weeks

Fig. 4 A map of cell fate decisions in fetal human frontal cortex.

a, Automated pairing of live and fixed samples and annotation of the video fields of view on the immunostained fixed samples. **b,** GFP+ cell matching between the live images and the fixed images. Arrowheads indicate equivalent cells. **c,** Live/fixed correlative analysis of a dividing bRG cell generating a bRG daughter and an IP daughter. **d,** Summary of all division patterns identified in bRG cells at GW 14 (N=170 bRG cells) and GW 18 (N=165 bRG cells) human frontal cortex. **e,** Percentage of proliferative versus neurogenic divisions of bRG cells in GW 14 and 18 human fetal tissue. **f,** Percentage of asymmetric (self-renewing) versus symmetric (self-consuming) neurogenic divisions of bRG cells in GW 14 and 18 human fetal tissue. **g,** Percentage of direct versus indirect neurogenic divisions of bRG cells in GW 14 and 18 human fetal tissue.

Figure 5

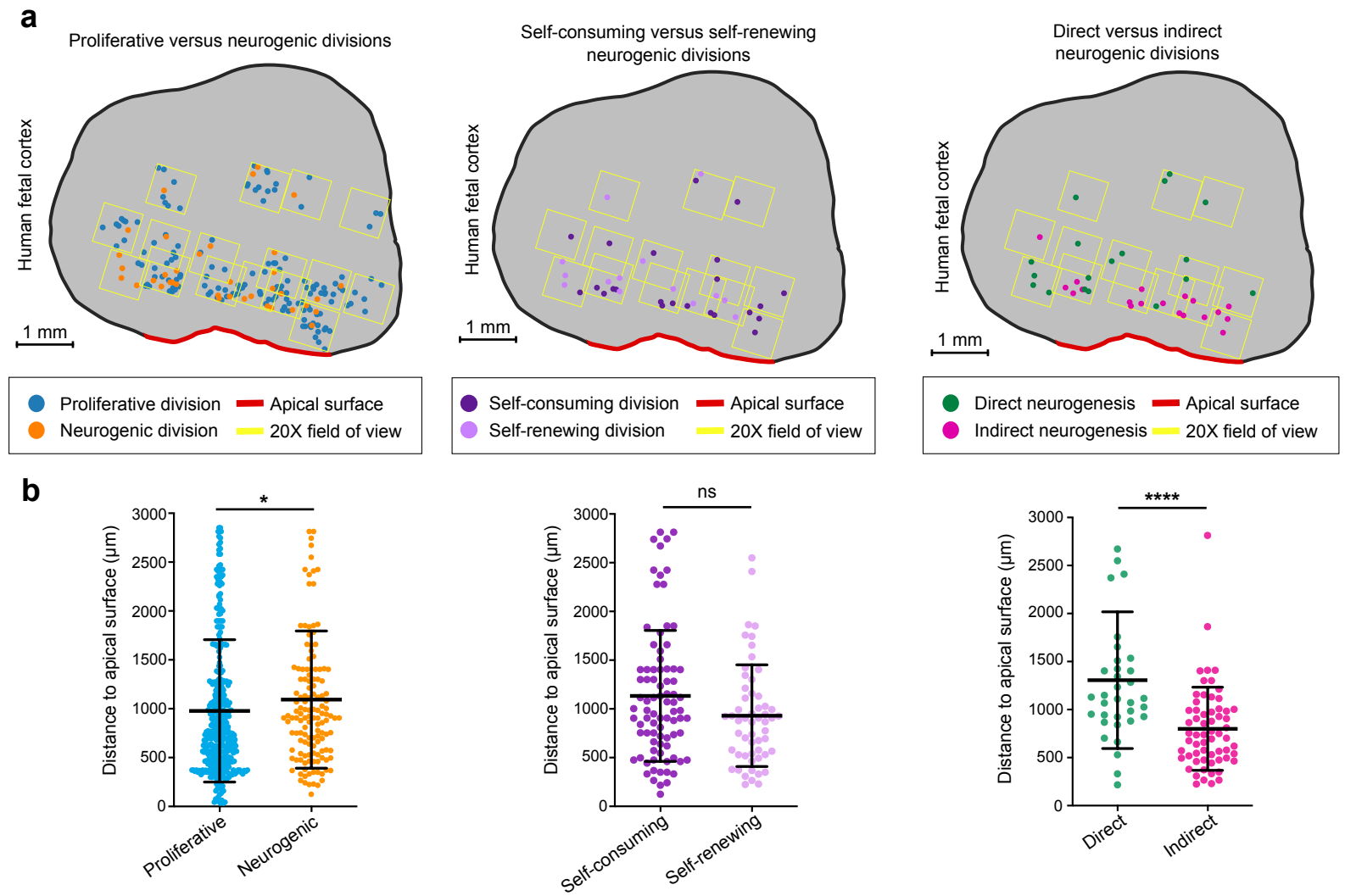
a
Proliferative versus neurogenic divisions
Self-consuming versus self-renewing neurogenic divisions
Direct versus indirect neurogenic divisions
Human fetal cortex
1 mm
Proliferative division
Neurogenic division
Apical surface
20X field of view
Self-consuming division
Self-renewing division
Direct neurogenesis
Indirect neurogenesis
b
Distance to apical surface (µm)
*
ns
****
Proliferative
Neurogenic
Self-consuming
Self-renewing
Direct
Indirect

Fig. 5 Spatial distribution of division modes in human fetal cortex.

a, Spatial distribution of proliferative versus neurogenic, self-consuming versus asymmetric self-renewing, and direct versus indirect neurogenic divisions in GW17 human frontal cortex. **b,** Quantification of proliferative versus neurogenic, self-consuming versus asymmetric self-renewing, and direct versus indirect neurogenic divisions in GW17-18 human frontal cortex. **(**N=355 cells for GW17 and 172 cells for GW18). All data are expressed as mean +/- standard deviation (SD). *p<0,05, ****p<0,0001 by two-tailed Mann-Whitney test.

Figure 6

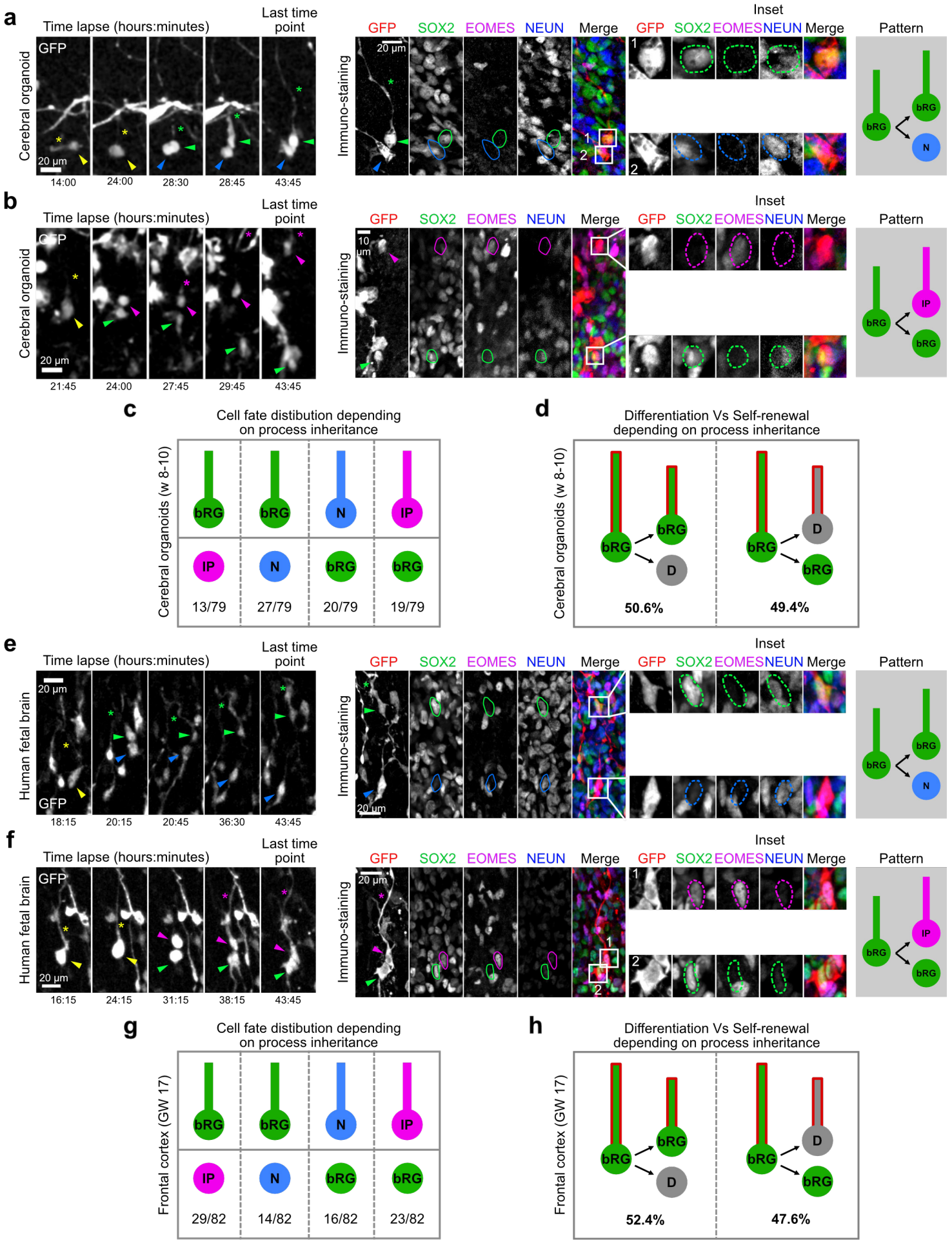
a
Time lapse (hours:minutes)
Last time point
GFP
Cerebral organoid
20 µm
14:00
24:00
28:30
28:45
43:45
Immuno-staining
GFP SOX2 EOMES NEUN Merge
Inset
GFP SOX2 EOMES NEUN Merge
Pattern
bRG
N
b
21:45
24:00
27:45
29:45
43:45
IP
c
Cell fate distibution depending on process inheritance
Cerebral organoids (w 8-10)
13/79
27/79
20/79
19/79
d
Differentiation Vs Self-renewal depending on process inheritance
D
50.6%
49.4%
e
Human fetal brain
18:15
20:15
20:45
36:30
43:45
f
16:15
24:15
31:15
38:15
43:45
g
Frontal cortex (GW 17)
29/82
14/82
16/82
23/82
h
52.4%
47.6%

Fig. 6 Basal process inheritance does not predict bRG fate upon asymmetric division.
a, Live/fixed correlative analysis of basal process inheritance in a dividing bRG cell generating a process-inheriting bRG daughter and neuron, within a cerebral organoid. **b,** Live/fixed correlative analysis of basal process inheritance in a dividing bRG cell generating a process-inheriting IP daughter and a bRG daughter, within a cerebral organoid. **c,** Distribution of cell fates depending on process inheritance upon asymmetric cell division in week 8-10 cerebral organoids (N=79 asymmetrically dividing cells from 5 experiments). **d,** Percentage of self-renewing versus differentiating daughter cells upon asymmetric division, depending on process inheritance in week 8-10 cerebral organoids (N=79 asymmetrically dividing cells from 5 experiments). **e,** Live/fixed correlative analysis of basal process inheritance in a dividing bRG cell generating a process-inheriting bRG daughter and a neuron, within fetal frontal cortex. **f,** Live/fixed correlative analysis of basal process inheritance in a dividing bRG cell generating a process-inheriting IP daughter and a bRG daughter, within fetal frontal cortex. **g,** Distribution of cell fates depending on process inheritance upon asymmetric cell division in GW 14-17 human frontal cortex (N=82 asymmetrically dividing cells from 2 experiments). **h,** Percentage of self-renewing versus differentiating daughter cells upon asymmetric division, depending on process inheritance in GW 14-17 human frontal cortex (N=82 asymmetrically dividing cells from 2 experiments).

Figure 7

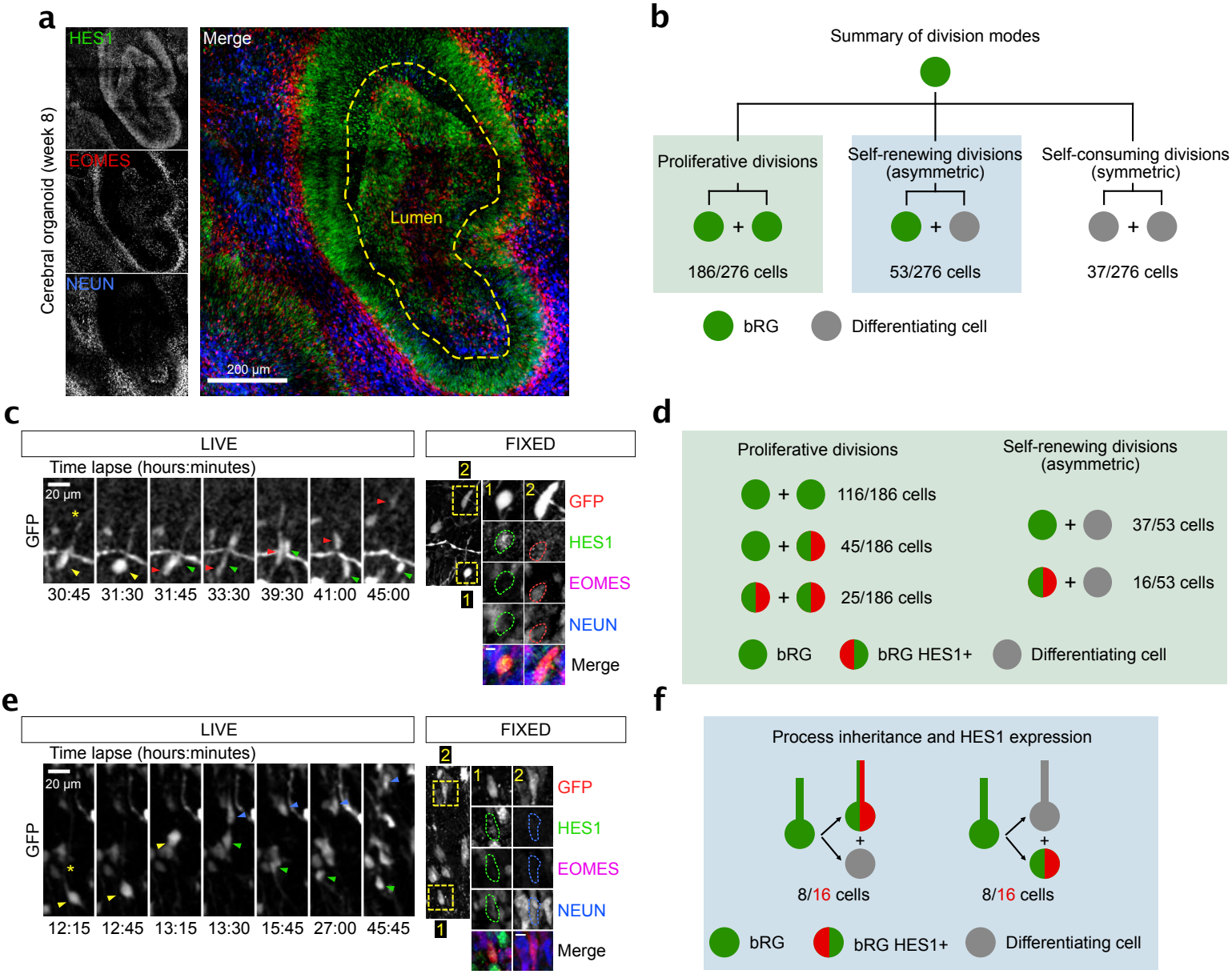
a
HES1
EOMES
NEUN
Cerebral organoid (week 8)
Merge
Lumen
200 µm
b
Summary of division modes
Proliferative divisions
186/276 cells
Self-renewing divisions (asymmetric)
53/276 cells
Self-consuming divisions (symmetric)
37/276 cells
bRG
Differentiating cell
c
LIVE
FIXED
Time lapse (hours:minutes)
20 µm
GFP
30:45
31:30
31:45
33:30
39:30
41:00
45:00
GFP
HES1
EOMES
NEUN
Merge
d
Proliferative divisions
116/186 cells
45/186 cells
25/186 cells
Self-renewing divisions (asymmetric)
37/53 cells
16/53 cells
bRG
bRG HES1+
Differentiating cell
e
LIVE
FIXED
Time lapse (hours:minutes)
20 µm
GFP
12:15
12:45
13:15
13:30
15:45
27:00
45:45
GFP
HES1
EOMES
NEUN
Merge
f
Process inheritance and HES1 expression
8/16 cells
8/16 cells
bRG
bRG HES1+
Differentiating cell

Fig. 7 HES1 is preferentially expressed in bRG daughters, irrespective of process inheritance.

a, HES1, EOMES and NEUN immunostaining in human cerebral organoid at week 8. **b,** Distribution of division modes identified in bRG cells within week 8-11 cerebral organoids. bRG daughter (EOMES- and NEUN-), differentiating daughter (EOMES+ or NEUN+) (N=276 bRG cells from 3 batches of organoids). **c,** Live/fixed correlative analysis of an asymmetrically dividing bRG cell revealing HES1 expression specifically in self-renewing daughter (EOMES- and NEUN-). **d,** Summary of HES1 expression in daughter cells depending on division modes (N= 239 cells from 3 batches of organoids). **e,** Live/fixed correlative analysis in asymmetrically dividing bRG cells revealing lack of correlation between HES1 expression and basal process inheritance. **f,** Summary of HES1 expression depending on process inheritance in asymmetrically dividing bRG cells, within week 8-11 cerebral organoids (N= 16 cells from 3 batches of organoids).

Figure S1

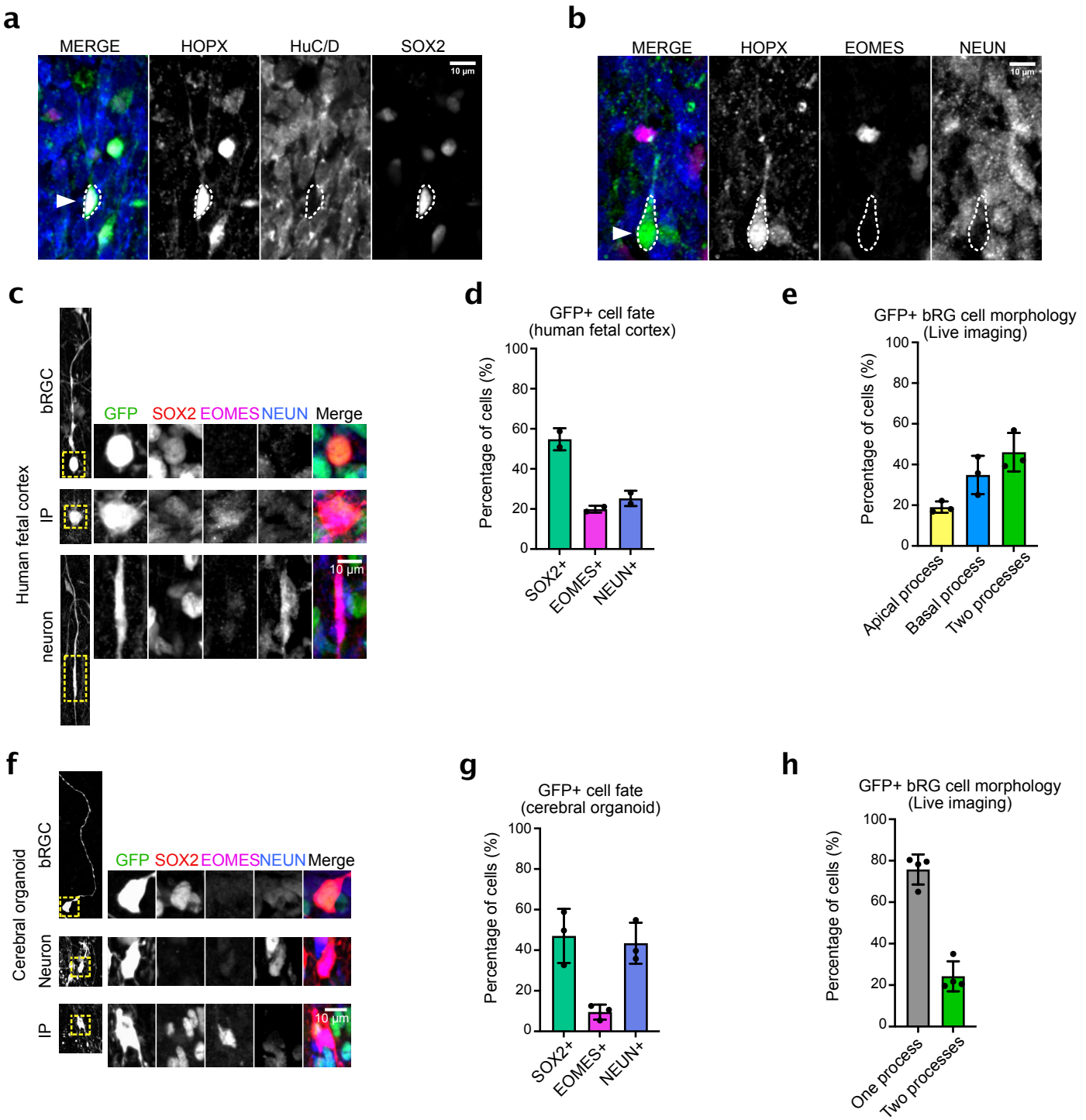
a
MERGE
HOPX
HuC/D
SOX2
10 μm
b
MERGE
HOPX
EOMES
NEUN
10 μm
c
Human fetal cortex
bRGC
IP
neuron
GFP
SOX2
EOMES
NEUN
Merge
10 μm
d
GFP+ cell fate
(human fetal cortex)
Percentage of cells (%)
100
80
60
40
20
0
SOX2+
EOMES+
NEUN+
e
GFP+ bRG cell morphology
(Live imaging)
Percentage of cells (%)
100
80
60
40
20
0
Apical process
Basal process
Two processes
f
Cerebral organoid
bRGC
Neuron
IP
GFP
SOX2
EOMES
NEUN
Merge
10 μm
g
GFP+ cell fate
(cerebral organoid)
Percentage of cells (%)
100
80
60
40
20
0
SOX2+
EOMES+
NEUN+
h
GFP+ bRG cell morphology
(Live imaging)
Percentage of cells (%)
100
80
60
40
20
0
One process
Two processes

Extended Data Fig. 1 Fate and shape of cells in cerebral organoids and fetal tissue.

a, Immunostaining for HOPX, HuC/D and SOX2 in human fetal cortex at GW18. **b**, Immunostaining for HOPX, EOMES and NEUN in human fetal cortex at GW18. **c**, Immunostaining for SOX2, EOMES and NEUN in GFP-infected human fetal cortex at GW17. **d,** Fate of GFP+ cells in human fetal cortex at GW 14-18. **e,** Morphology of GFP+ bRG cells in live imaged human fetal samples at GW 14-18. **f,** Immunostaining for SOX2, EOMES and NEUN in GFP-infected cerebral organoids at week 8. **g,** Fate of GFP+ cells in cerebral organoids at week 8-10. **h,** Morphology of GFP+ bRG cells in live imaged cerebral organoids at week 8-10.

Figure S2

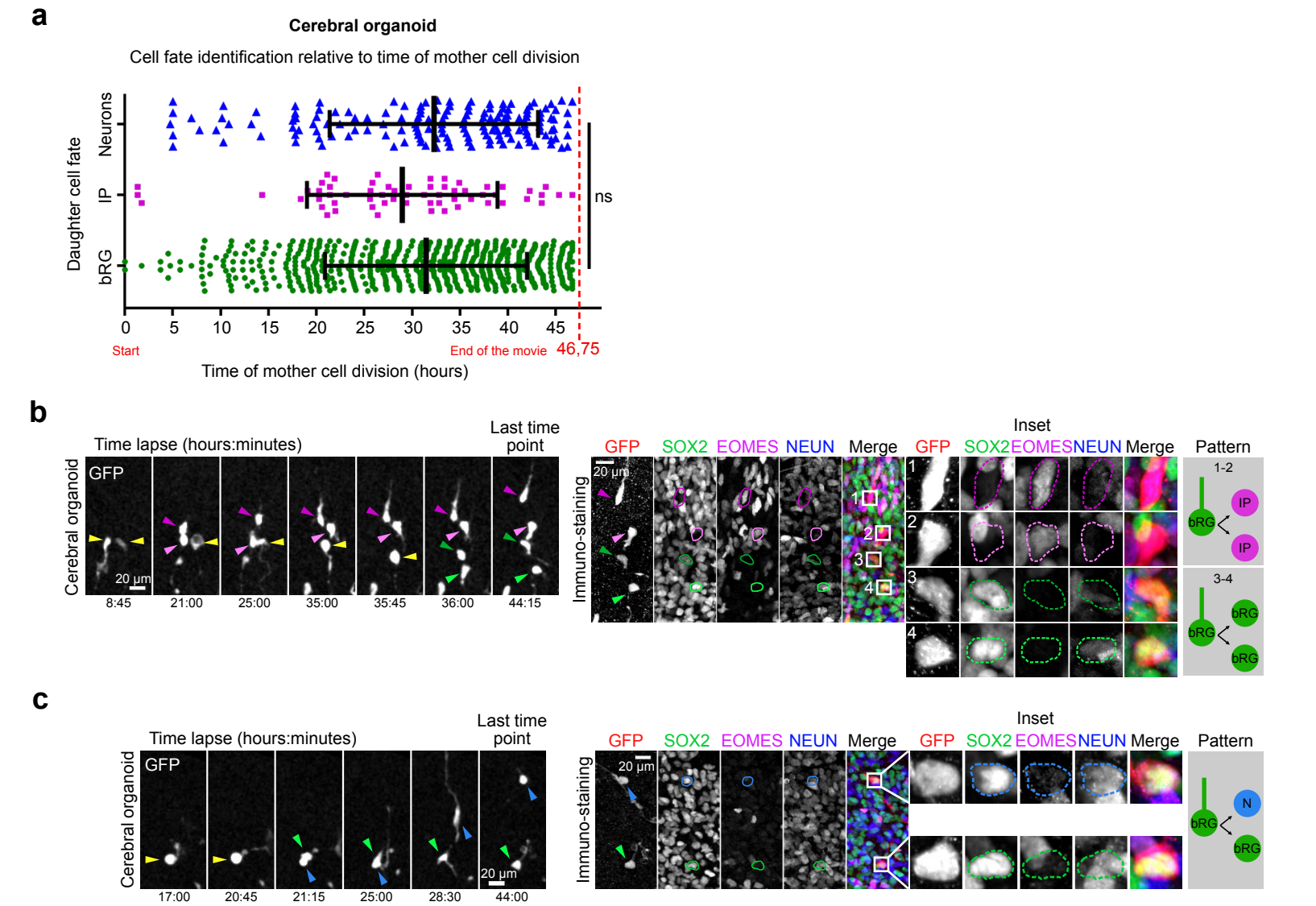
a
Cerebral organoid
Cell fate identification relative to time of mother cell division
Daughter cell fate
Neurons
IP
bRG
ns
0
5
10
15
20
25
30
35
40
45
Start
End of the movie
46,75
Time of mother cell division (hours)
b
Time lapse (hours:minutes)
Last time point
Cerebral organoid
GFP
20 µm
8:45
21:00
25:00
35:00
35:45
36:00
44:15
Immuno-staining
GFP
SOX2
EOMES
NEUN
Merge
Inset
Pattern
1-2
3-4
IP
bRG
c
Time lapse (hours:minutes)
Last time point
Cerebral organoid
GFP
20 µm
17:00
20:45
21:15
25:00
28:30
44:00
Immuno-staining
GFP
SOX2
EOMES
NEUN
Merge
Inset
Pattern
N
bRG

Extended Data Fig. 2 Live/fixed correlative examples and cell fate identification timing in cerebral organoids.

a, Detection of bRG, IP or neuronal cell fate relative to the time of division of the bRG mother cell in cerebral organoids at week 8-10. **b,** (Top) Live/fixed correlative analysis of a dividing bRG cell generating two IP daughters. (Bottom). Live/fixed correlative analysis of a dividing bRG cell generating two bRG daughters. **c**, Live/fixed correlative analysis of a dividing bRG cell generating a bRG daughter and a neuronal daughter.

Figure S3

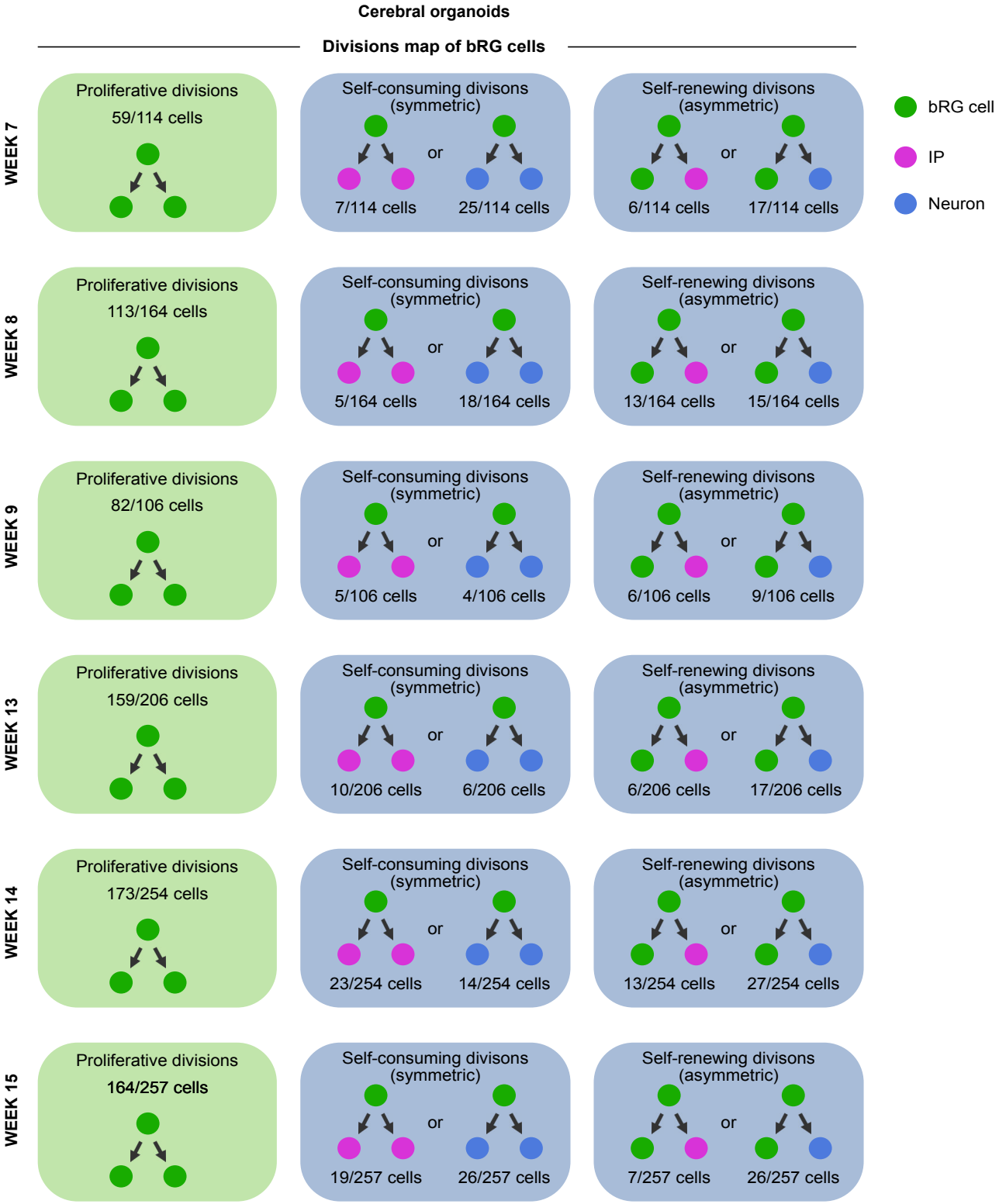
Cerebral organoids
Divisions map of bRG cells
WEEK 7
Proliferative divisions
59/114 cells
Self-consuming divisons
(symmetric)
or
7/114 cells
25/114 cells
Self-renewing divisons
(asymmetric)
or
6/114 cells
17/114 cells
WEEK 8
Proliferative divisions
113/164 cells
Self-consuming divisons
(symmetric)
or
5/164 cells
18/164 cells
Self-renewing divisons
(asymmetric)
or
13/164 cells
15/164 cells
WEEK 9
Proliferative divisions
82/106 cells
Self-consuming divisons
(symmetric)
or
5/106 cells
4/106 cells
Self-renewing divisons
(asymmetric)
or
6/106 cells
9/106 cells
WEEK 13
Proliferative divisions
159/206 cells
Self-consuming divisons
(symmetric)
or
10/206 cells
6/206 cells
Self-renewing divisons
(asymmetric)
or
6/206 cells
17/206 cells
WEEK 14
Proliferative divisions
173/254 cells
Self-consuming divisons
(symmetric)
or
23/254 cells
14/254 cells
Self-renewing divisons
(asymmetric)
or
13/254 cells
27/254 cells
WEEK 15
Proliferative divisions
164/257 cells
Self-consuming divisons
(symmetric)
or
19/257 cells
26/257 cells
Self-renewing divisons
(asymmetric)
or
7/257 cells
26/257 cells
bRG cell
IP
Neuron

Extended Data Fig. 3 Cell fate decision patterns in W7-15 cerebral organoids.

Summary of all division patterns identified in bRG cells in week 7, 8, 9, 13, 14 and 15 cerebral organoids. Week 7 (N=114 bRG cells), week 8 (N=164 bRG cells), week 9 (N=106 bRG cells), week 13 (N=206 bRG cells), week 14 (N=254 bRG cells) and week 15 (N=257 bRG cells).

Figure S4

a

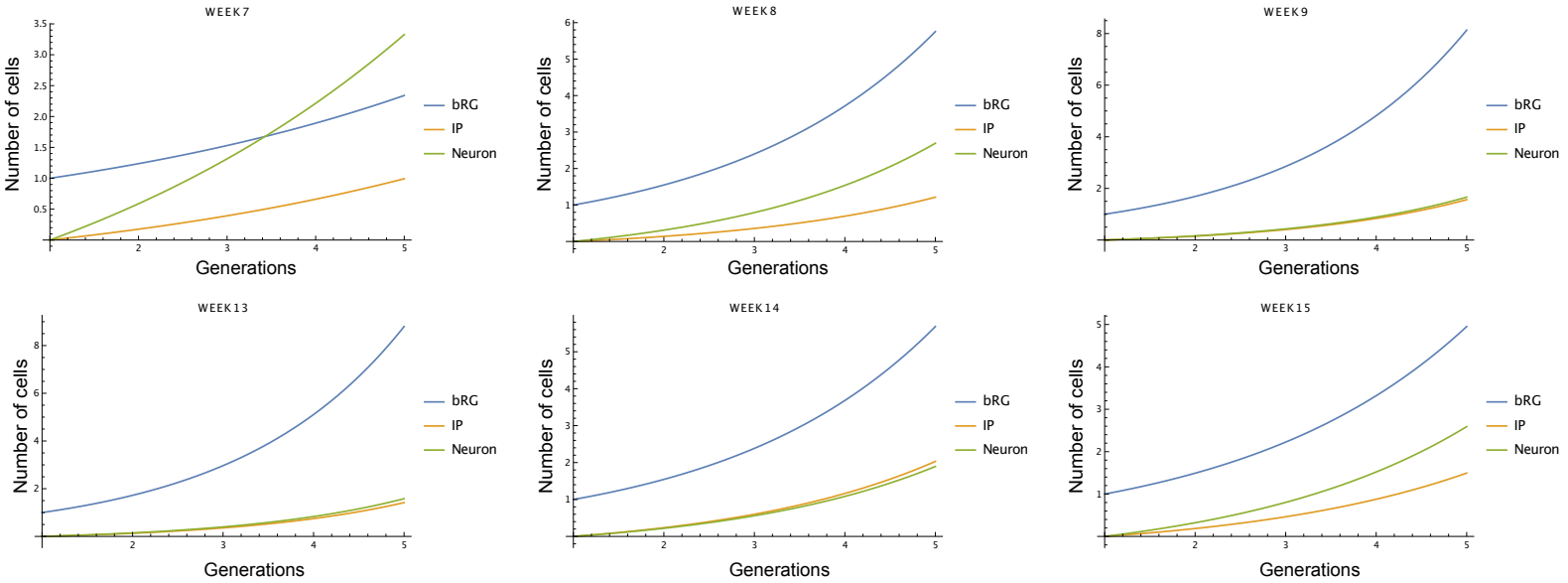
WEEK7
WEEK8
WEEK9
WEEK13
WEEK14
WEEK15
Number of cells
Generations
bRG
IP
Neuron

b

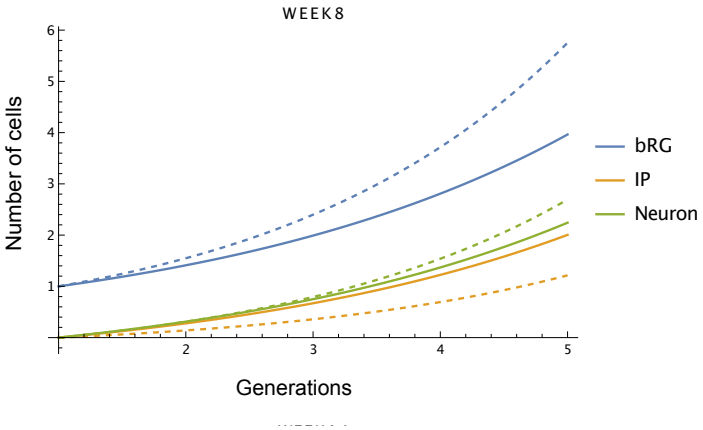
WEEK8
Number of cells
Generations
bRG
IP
Neuron

Extended Data Fig. 4 bRG cells output in week 7-15 cerebral organoids.

a, Simulation of the output of a single bRG cell after 1-5 generations, in week 7-9 and 13-15 cerebral organoids. **b**, Simulation of the output of a single bRG cell after 1-5 generations in week 8 cerebral organoids (dashed lines) compared to the output of a single bRG cell that underwent 20% less symmetric amplifying divisions in favor of asymmetric indirect divisions (full lines).

Figure S5

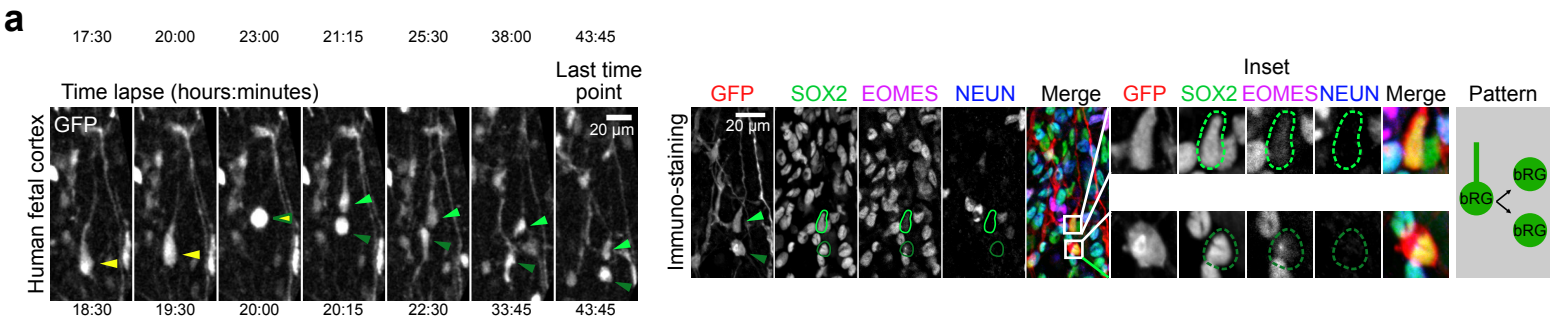
a
17:30
20:00
23:00
21:15
25:30
38:00
43:45
Time lapse (hours:minutes)
Last time point
Human fetal cortex
GFP
20 µm
18:30
19:30
20:00
20:15
22:30
33:45
43:45
Inset
GFP
SOX2
EOMES
NEUN
Merge
Pattern
Immuno-staining
bRG

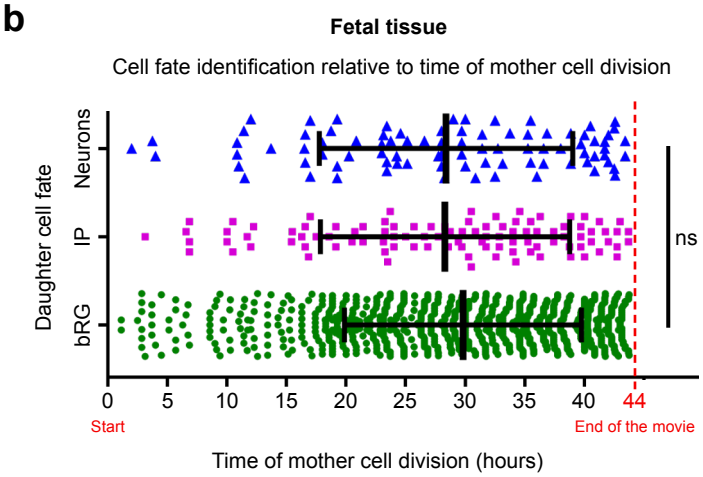
b
Fetal tissue
Cell fate identification relative to time of mother cell division
Daughter cell fate
Neurons
IP
bRG
ns
0
5
10
15
20
25
30
35
40
44
Start
End of the movie
Time of mother cell division (hours)

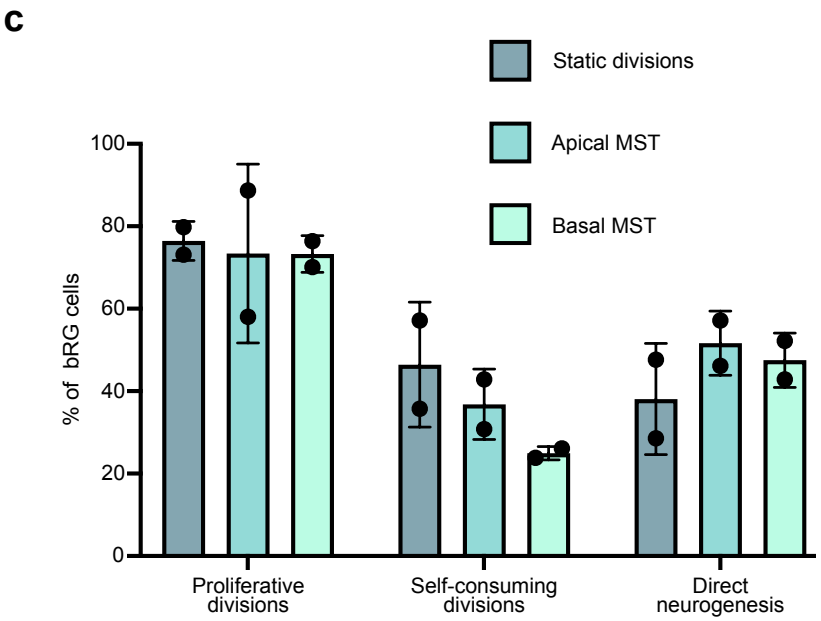
c
Static divisions
Apical MST
Basal MST
% of bRG cells
100
80
60
40
20
0
Proliferative divisions
Self-consuming divisions
Direct neurogenesis

Extended Data Fig. 5 Cell fate identification timing in fetal tissue.

a, Live/fixed correlative analysis of a dividing bRG cell generating two bRG daughters. **b,** Detection of bRG, IP or neuronal cell fate relative to the time of division of the bRG mother cell in human fetal samples at GW 14-18. **c,** Percentage of bRG cells performing proliferative divisions, of neurogenic bRG cells performing self-consuming divisions and of neurogenic bRG cells performing direct neurogenic divisions, depending on their division mode (static, apical MST or basal MST).

Figure S6

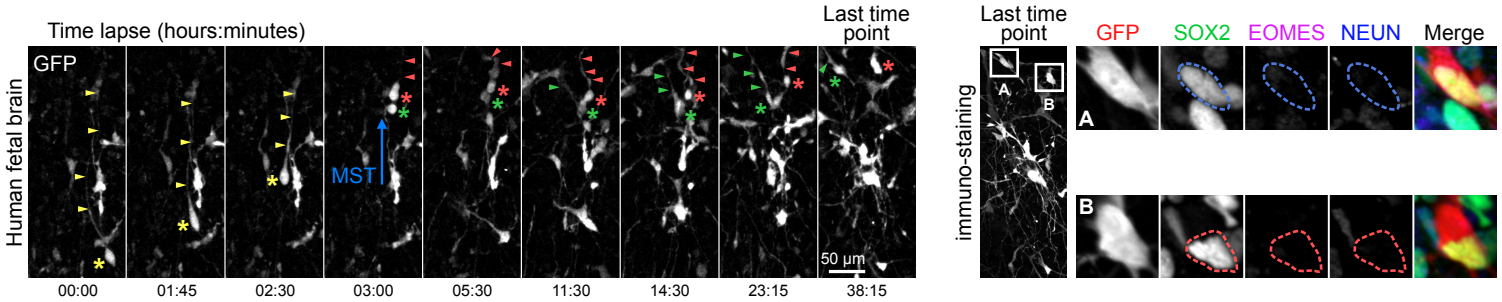
Time lapse (hours:minutes)
Last time point
GFP
Human fetal brain
MST
50 µm
00:00
01:45
02:30
03:00
05:30
11:30
14:30
23:15
38:15
Last time point
GFP
SOX2
EOMES
NEUN
Merge
immuno-staining
A
B

Extended Data Fig. 6 SOX2+ bRG daughter cells regrow a basal process if at birth.

A. Live/fixed correlative analysis of a dividing bRG cell generating two bRG daughters. Asterix indicates cell soma and arrowhead indicates basal process. Mother cell (yellow) divides into a process-inheriting cell (red) and a cell that regrows a basal process (green).

Figure S7

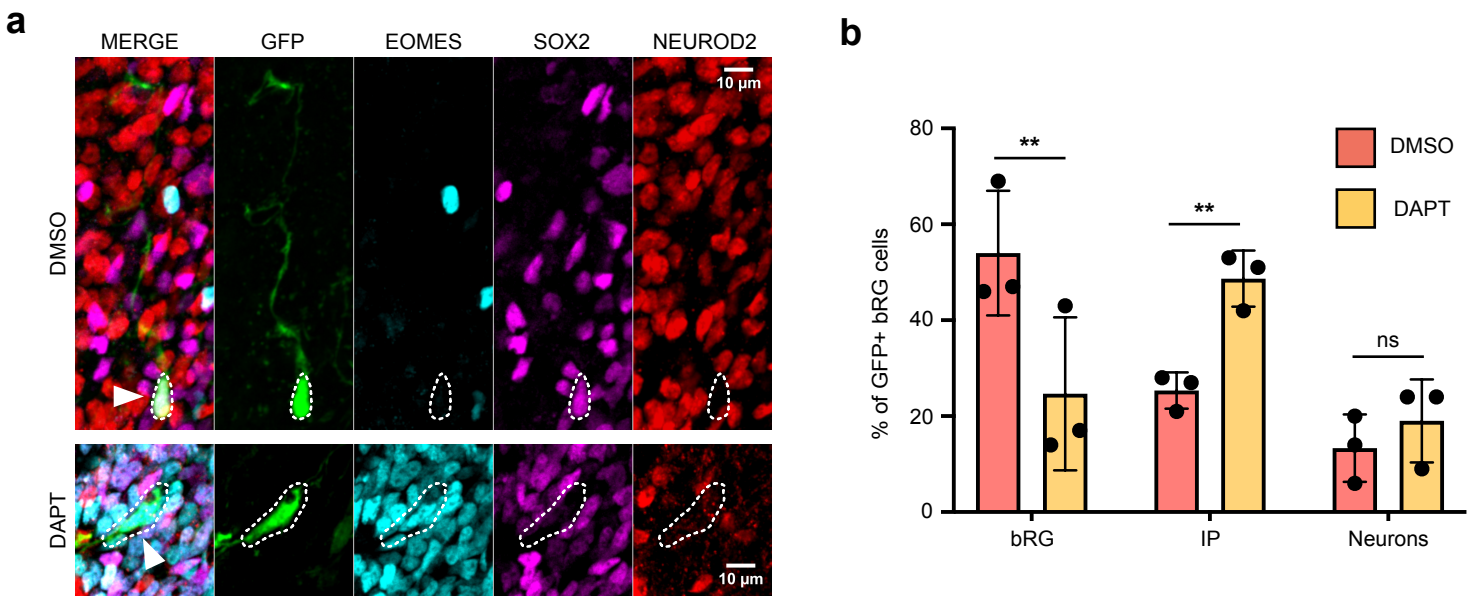
a
MERGE
GFP
EOMES
SOX2
NEUROD2
DMSO
DAPT
10 µm
10 µm
b
% of GFP+ bRG cells
80
60
40
20
0
**
**
ns
DMSO
DAPT
bRG
IP
Neurons

Extended Data Fig. 7 NOTCH inhibition induces RG depletion and IP generation.

a, Immunostaining for SOX2, EOMES and NEUROD2 in GFP-infected week 8 cerebral organoids, following incubation with DMSO or 5μM DAPT for 48 hours. **b**. Percentage of bRG (SOX2+), IPs (EOMES+) and Neurons (NEUROD2+) newborn GFP+ cells after 48 hour treatment with DMSO or 5μM DAPT. All data are expressed as mean +/- standard deviation (SD). **p<0,01, by two-tailed t-test.